Development patterns of an isolated oligo-mesophotic carbonate buildup, early Miocene, Yadana field, offshore Myanmar

Thomas Teillet, François Fournier, Lucien F. Montaggioni, Marcelle Boudagher-Fadel, Jean Borgomano, Juan Braga, Quentin Villeneuve, Fei Hong

Development patterns of an isolated oligo-mesophotic carbonate buildup, early Miocene, Yadana field, offshore Myanmar

Thomas Teillet [1,2], François Fournier [1], Lucien F. Montaggioni [1], Marcelle BouDagher-Fadel[3], Jean Borgomano [1], Juan C. Braga [4], Quentin Villeneuve [1], Fei Hong [2]

[1] : Aix Marseille Univ, CNRS, IRD, Coll France, CEREGE, 3 Place Victor Hugo, Case 67, 13331 Marseille Cedex 03, France

[2]: TOTAL, CSTJF, Avenue Larribau, 64018 Pau Cedex, France

[3]: Postgraduate Unit of Micropalaeontology, Department of Geological Sciences, University College London, Gower Street, London WC1E 6BT, U.K.

[4] : Departamento de Estratigrafía y Paleontología, Universidad de Granada, Campus Fuente Nueva 18002 Granada, Spain

Abstract

The development history of an oligo-mesophotic, early Miocene, isolated carbonate system (>160 m in thickness), forming the uppermost part of the Oligo-Miocene Yadana buildup (northern Andaman Sea), has been evidenced from the integration of sedimentological core studies from 4 wells (cumulated core length: 343 m), well correlations, seismic interpretation and

analysis of the ecological requirements of the main skeletal components. Three types of carbonate factory operated on the top of the platform, depending on water-depth, turbidity and nutrient level: (1) a scleractinian factory developing under mesophotic conditions during periods of high particulate organic matter supplies, (2) an echinodermal factory occupying dysphotic to aphotic area of the platform coevally with the scleractinian factory, (3) a large benthic foraminiferal-coralline algal factories prevailing under oligo-mesophotic and oligo-mesotrophic conditions. The limited lateral changes in facies between wells, together with the seismic expression of the Yadana buildup, suggest deposition on a flat-topped shelf. Carbonate production and accumulation on the Yadana platform was mainly controlled by light penetration, nutrient content and hydrodynamic conditions. Scleractinian-rich facies resulted from transport of coral pieces derived from mesophotic environments (mounds?) and deposited in deeper, low light, mud-rich environments in which lived abundant communities of suspension feeders such as ophiuroids. Changes in monsoonal intensity, terrestrial runoff from the Irrawaddy River, upwelling currents and internal waves activity during the early Miocene are likely responsible for significant variations in water turbidity and nutrient concentration in the Andaman Sea, thus promoting the development of an oligo-mesophotic, incipiently drowned platform.

Key-words: Miocene, carbonate buildup, oligophotic, mesophotic, large benthic foraminifera, coralline algae, corals, Yadana.

1. Introduction

Prolific literature devoted tropical Cenozoic carbonate systems from Southeast Asia reveals a great diversity of carbonate factories in relation to a wide range of global and local environmental and climatic parameters, including temperature, nutrient content, light penetration and terrigenous inputs (e.g., Wilson, 2002; Wilson and Vecsei, 2005; Madden and Wilson, 2013; Nowak et al., 2013; Santodomingo et al., 2015). Usually, the concept of 'tropical carbonate factory' is associated with a dominantly biological carbonate production in warm, well-illuminated, oligotrophic, and very shallow waters (e.g., Hallock and Glenn, 1986; Schlager, 2000, 2003; Pomar and Hallock, 2008). In such settings, carbonates are typically produced by various photosynthetic autotrophs including calcareous green and red algae, and by symbiont-bearing organisms such as zooxanthellate corals and large benthic foraminifera, thus resulting in the so-called photozoan sediment association (James, 1997). These humid tropical environments may be affected by a wide range of siliciclastic, fresh water and nutrients inputs that are generally considered to be unfavorable to the photozoan carbonate production (e.g., Wilson, 2002, 2008). Many modern and Cenozoic equatorial, southeast Asian carbonate systems are associated with upwelling and/or terrestrial runoff, high turbidity and cool waters (Madden and Wilson, 2013). In such settings, nutrient-reliant biota often outweighs light dependent autotrophs (Tomascik et al., 2000; Wilson and Vecsei, 2005). At a regional scale, the combined effect of high nutrient supplies and low light penetration promotes the development of large scale isolated and/or land-attached oligophotic (*sensu* Pomar, 2001) platforms such as the modern Paternoster Platform (Burollet et al., 1986), Spermonde Platform (Renema and Troelstra, 2001), Kalukalukung Banks (Roberts and Phipps, 1988) and the Cenozoic Berai (Saller and Vijaya, 2002), Tonasa (Wilson and Bosence, 1996), Melinau platforms (Adams, 1965) and foreslope of Hawaiian Islands (Pyle et al., 2016). However in such carbonate platforms, even though

70 oligophotic carbonate production dominates, reefal and/or non-reefal euphotic carbonate factories are coexisting (Wilson and Vecsei, 2005). The reconstruction of depositional models
72 for ancient, coral-rich sedimentary systems has become a major issue in carbonate sedimentology since significant oligo-mesophotic scleractinian carbonate factories have been
74 evidenced in modern and Cenozoic environments (e.g., Lesser et al., 2009; Kahng et al. 2010; Morsilli et al. 2012), thus questioning the common use of 'tropical carbonate factory' concepts in
76 paleoenvironmental interpretations.

The late Oligocene- early Miocene Yadana carbonate platform is located in the Andaman Sea,
78 offshore Myanmar (Fig. 1A). Three-dimensional seismic interpretation of the Yadana gas-bearing carbonate reservoir revealed that towards the upper part of the Yadana limestones
80 (Upper Burman Limestone), the platform is transitioning from an attached to an isolated configuration (Paumard et al., 2017). The analysis of seismic facies coupled with the use of
82 modern analogues of tropical carbonate systems have led to interpret the Yadana buildup as a euphotic reef-rimmed carbonate platform (Paumard et al., 2017). The present study, on the basis
84 of a detailed analysis of biological associations, sedimentological and diagenetic features from cores, aims at (1) revisiting the depositional model of the Upper Burman Limestone, previously
86 established by Paumard et al. (2017), (2) assessing the impact of environmental factors such as turbidity, light penetration, hydrodynamic energy and nutrient availability on carbonate
88 production in tropical isolated carbonate platforms, (3) documenting the development of a coral-rich isolated carbonate system in mesophotic conditions, in southeast Asia during the early
90 Miocene, and 4) linking changes in environmental conditions and carbonate production with the stratigraphic architecture of an isolated carbonate buildup with dominant oligo-mesophotic
92 production. Such depositional models are also relevant in oil and gas industry since they may

constrain the exploration targets and production strategies in carbonate settings with dominant oligo-mesophotic contribution.

.

2. Geological setting

During the Cenozoic, the regional geodynamic context strongly controlled the initiation, the development and the demise of southeast Asian carbonate systems (Wilson and Hall, 2010). As a result of the oblique collision of the Indian-Australian plate beneath the Eurasian plate, the Sunda subduction zone formed during the early Eocene (Curray, 2005; Chakraborty and Khan, 2009), and induced the opening of the Andaman Sea as a back-arc basin. During the late Oligocene to the early Miocene (Fig. 2), the Yadana carbonate buildup, 25 km to 30 km in size, developed at the top of a volcanic basement, located in the northern Andaman Sea (Racey and Ridd, 2015; Paumard et al., 2017). The volcanic basement has been interpreted as a volcanic arc separating the M5 fore-arc basin to the west from the Moattama back-arc basin to the east (Racey and Ridd, 2015) or alternatively as a volcanic ridge, created during the northward motion of the Indian plate above the Kerguelen island hotspot (Paumard et al., 2017) (Fig. 2).

Paumard et al. (2017) proposed a review of the stratigraphy and age of the Yadana carbonate platform based on a regional study integrating seismic and well data. The lowermost deposits from the Moattama Basin (Fig. 3) consists of Upper Eocene volcano-clastics sediments. The overlying Oligo-Miocene shallow-water carbonates may reach up to 700 m in thickness, and are subdivided into two distinct formations: the Lower Burman Limestone, and the Upper Burman

Limestone. The Lower Burman Limestone, Chattian in age is composed of two distinct carbonate buildups separated by a SW-NE-trending trough which is filled by the Sein Clastics Formation (late Chattian). The overlying Upper Burman Limestone has been interpreted as recording an upward transition from an attached platform to a single, reef-rimmed isolated carbonate buildup during the early Miocene. At the end of the Upper Burman Limestone deposition, a long-term depositional hiatus occurred from the early Miocene to the late Miocene. The Upper Burman Limestone carbonates are sealed by late Miocene (N16 planktonic zone) shales (Pyawbwe and Badamyar formations) from the Irrawaddy deltaic system. A major eastward tilting phase of the Yadana platform, evidenced by seismic profiles (Fig. 2), occurred during the late Miocene (horizon M6: 8.2 Ma, after Paumard et al., 2017).

3. Material and Methods

Approximately 20 wells have penetrated the top of the Upper Burman Limestone. Four wells (WELL-1, WELL-2, WELL-3 and WELL-4), located in the western half of the buildup (Fig. 2B), have been selected in this study for a detailed sedimentological study, totalizing 343 m of cumulated length (WELL-1: 87.5 m, WELL-2: 84 m WELL-3: 59.5 m WELL-4: 112 m). The carbonate interval penetrated by cores averages 160 meters.

Macroscopic core description and thin-section study under polarized-light microscopy provided the sedimentologic framework for the present study. Around 700 thin sections were prepared from cores with an average spacing of 0.5 m and stained with red alizarin and potassium ferrocyanide.

All thin sections were point counted on the basis of 300 points to quantify the bioclastic composition of the carbonates. Lithofacies have been defined based on sedimentary structures, depositional textures and biological composition identified from cores and thin-sections. These lithofacies have been interpreted in terms of depositional environments by reference to modern and ancient analogues. The paleoenvironmental reconstructions have been constrained using light-dependent communities including coralline algae and large benthic foraminifera. Bathymetric zonation is based on the distinction between "euphotic" (maximal light intensity commonly associated with high wave energy), "mesophotic" (sufficient light for coral development, typically below normal wave base), "oligophotic" (sufficient light for coralline algae), and "dysphotic" (insufficient light for photosynthesis) and "aphotic" (Pomar, 2001).

The chronostratigraphic framework of the Yadana carbonate buildup has been revisited (Fig. 4) on the basis of: (1) a reappraisal of the available planktonic and benthic foraminiferal biostratigraphy, and (2) new taxonomic determinations of the benthic foraminiferal material from the studied Upper Burman Limestone cores (Fig. 5). The benthic foraminiferal stratigraphy was based on the East Indian Letter Classification (Adams, 1970; BouDagher-Fadel, 1999; BouDagher-Fadel, 2015, 2018) and planktonic foraminiferal biostratigraphy on the zonation defined by Berggren et al. (1995) and modified by Wade et al. (2011), by using the time scale defined by Gradstein et al. (2012).

The correlation framework between wells has been defined on the basis of: (1) biostratigraphic constraints, and (2) correlation of vertical changes in light penetration and trophic conditions.

The studied dataset includes 2D and 3D seismic surveys acquired by TOTAL. The 2D seismic profiles were acquired between 1993 and 1997 cover an area of ~14 200 km2. The 3D seismic

164 data were acquired in 2011, over area of ~511 km2. The 3D volume is characterized by a bin spacing of 12.5 x 6.25 m and a trace sampling of 3 ms. The vertical resolution of the prestack
166 time migrated data used in the present work is around 20 m within the carbonate reservoir. In addition to the gas water contact (GWC), that forms a well-identified flat-spot, five seismic
168 reflectors (TOP UBL, H9, H9A, H10B and H10), have been interpreted throughout the carbonate buildup from 3D seismic data.

170

172

4. Results

174

176 ### *4.1 Biostratigraphy*

178 The Upper Burman Limestone overlies the Sein siliciclastics of late Rupelian to early Chattian age as derived from the occurrence of *Paragloborotalia opima* (P20-P21). The age of the lower
180 part of the UBL limestones (below the cored interval) is poorly constrained. The lowermost cored interval from the Upper Burman Limestone is early Aquitanian in age (N4a) as supported
182 by the first co-occurrence of *Miogypsinella ubaghsi* (Fig. 5 A) and *Miogypsinoides formosensis* (WELL-1, 1340.06 m). Above, the co-occurrence of *Miogypsinoides bantamensis* (Fig. 5 C) and
184 *Miogypsina gunteri* indicates a later Aquitanian age (N4). The uppermost Upper Burman Limestone is recognized to be Burdigalian in age (N6) on the basis of the occurrence of
186 *Miogypsina intermedia* (Fig. 5 B), *Miogypsina globulina* and *Miogypsinoides dehaarti* (WELL-2 1272.23 m).

188 Calcareous nannofossils and planktonic foraminifers present in the shales overlying the UBL (*Discoaster quinqueramus*, *Sphaeroidinellopsis seminulina*, *Globigerinoides extremus*) are

assigned to the Tortonian (N20-N17), thus suggesting a hiatus duration of approximatively 9 My at top of the Yadana platform (Burdigalian-Tortonian hiatus)

4.2 Lithofacies and paleo-environmental interpretations

Carbonates from the UBL interval are calcite-dominated limestones, with few partially dolomitized intervals. In decreasing order of abundance the main biological components observed on thin sections are: (1) non-geniculate coralline algae (42% of total bioclastic fraction on average; WELL-1=48%; WELL-2=41%; WELL-3=45%; WELL-4=33%), (2) larger benthic foraminifera (41% on average; WELL-1=38%; WELL-2=42% ; WELL-3=41%; WELL-4=41%) and (3) corals (16% on average; WELL-1=8%; WELL-2=20%; WELL-3=12%; WELL-4=25%). Subordinate components include echinoderms (5% on average), bryozoans, green algae and planktonic foraminifera. Five distinct lithofacies have been defined and interpreted in terms of depositional environments (Table 1):

LF1. Coralline algal floatstone to rudstone

The coralline algal floatstones to rudstones (Fig. 6 A-G) consist of spheroidal-ellipsoidal rhodoliths or pieces of branching coralline algae embedded within a coralline algal-foraminiferal wackestone to packstone matrix. The coralline algal association is composed of *Lithothamnion, Mesophyllum* and *Sporolithon.* Rhodoliths are heterometric, mostly with diameters ranging from 1 cm to 10 cm in cores and commonly displaying warty and branching growth forms. Loose pieces of branching and columnar (fruticose) coralline algae (particularly *Lithothamnio*n and *Sporolithon*) may be dominant in some intervals (Fig. 6C, D). Loose and hooked *Mesophyllum* are present in very low amount (Fig. 6F). Mastophoroids are

214 extremely rare or lacking. The foraminiferal assemblage is dominated by *Spiroclypeus tidoenganensis* and *Nephrolepidina sumatrensis*, with common occurrences of
216 *Miogypsinoides*, *Miogypsina* and *Heterostegina* (*Vlerkina*). Echinoderms, ectoprocts and planktonic foraminifera are occasional.

218 **Interpretation**: In LF1 facies, the coralline algal assemblage is dominated by the melobesioids *Lithothamnion*, *Mesophyllym* and *Sporolithon.* Such an assemblage is typical of
220 low-light environments, in oligo-mesophotic settings (Braga et al., 2010). In modern, tropical, low-turbidity environments, melobesioids have been shown to occur preferentially
222 at water-depths ranging from 30 to 80 m (Adey, 1979; Braga and Aguirre, 2004). The co-occurrence of warty rhodoliths and pieces of branching coralline algae belonging to the same
224 taxa (Fig. 6C, G) may suggest that the isolated branches may derive from the fragmentation of branching rhodoliths during high-energy events (Bosence, 1983; Freiwald et al., 1994),
226 such as storms, cyclones or internal waves. The foraminiferal assemblage dominated by large and flat *Spiroclypeus* and Lepidocyclinids is typical of oligo-mesophotic environments, at
228 water depths of 30 m or greater, but could live comfortably at 70 m depth (Hallock and Glenn, 1986; Noad, 2001). In contrast, benthic foraminifers like *Miogypsinoides*, *Miogypsina*
230 and *Heterostegina* (*Vlerkina*) are common taxa in shallow-water, euphotic environments associated with sea-grass beds (Fournier *et al.*, 2004; BouDagher-Fadel, 2018; Hallock and
232 Pomar, 2008; Maurizot *et al*., 2016) but were also reported from shallow mesophotic, mid-ramp environments (Bassi, 2005; Bassi *et al.*, 2007; Rahmani *et al.,* 2009). The mud-
234 supported nature of LF1 suggests that the depositional environment was relatively sheltered or not permanently subject to wave action. As a consequence, the biological and textural
236 features of LF1 facies likely reflect deposition in the shallowest part of the mesophotic zone,

in an area located below the base of fair-weather wave action but experiencing episodic high-
238 energy events.

240 **LF2.1. Large benthic foraminiferal rudstone**

The LF2.1 facies (Fig. 7A, B) consists of relatively thin (< 1 m) accumulations of large benthic
242 foraminifers, enriched in red algal fragments, with rare bryozoans and echinoderms which are typically interbedded within coralline algal floatstones (LF1). The intergranular spaces may be
244 occupied by a peloidal grainstone matrix or occluded by sparry calcite cements. Large benthic foraminifera are usually centimetric in size (sometimes up to 2 cm) and most of them display
246 broken edges. The foraminiferal assemblage is dominated by *Lepidocyclina* (*Nephrolepidina*) *sumatrensis*, *L.* (*N.*) *oneatensis,* and *Spiroclypeus tidoenganensis* with rarer specimens of
248 *Amphistegina*, *Heterostegina*, *Miogyspina,* and *Miogypsinoides*. Coralline algae mainly include branching and encrusting, warty *Lithothamnion*, laminated, loose *Mesophyllum* and branching
250 *Sporolithon.* The LF2.1 rudstone intervals exhibit close (cm- scale) vertical and lateral orientation changes of large benthic foraminifera (Fig. 7B).

252 **Interpretation**: The foraminiferal assemblage, dominated by *Nephrolepidina* and *Spiroclypeus* as well as the coralline algal association (*Lithothamnion-Mesophyllum-Sporolithon*) suggest that
254 carbonate grains have been produced within the mesophotic zone (Braga et al., 2010). In addition, the lack or scarcity of mud matrix in intergranular spaces, with the poor state of
256 preservation of large benthic foraminifers, may indicate that frequent turbulence was strong enough to winnow muddy particles and rework the large foraminiferal tests. The rare occurrence
258 of *Amphistegina*, *Heterostegina*, *Miogyspina,* and *Miogypsinoides,* compared to LF1, may reflect that the sediment source of the rudstones is located at greater depths within the mesophotic zone

but may also give evidence of preferential sorting of low-density bioclasts such as large and flat lepidocyclinids and *Spiroclypeus* (Jorry et al., 2006; Pomar et al., 2012; 2015). The low intergranular matrix content and predominantly non-oriented nature of the large benthic foraminifera in LF2.1 is interpreted as resulting from a bedload transportation and mass deposition during high-energy events (storms or internal waves). In addition, the occurrence of LF2.1 rudstone beds within mesophotic LF1 coralline algal and foraminiferal floatstones, together with the mesophotic affinity of the biotic assemblage in LF2.1 also indicates that during high-energy events the sediment was remobilized and then redeposited on top of the Yadana shelf in a similar water-depth range.

LF2.2. Large benthic foraminiferal floatstone

LF2.2 lithofacies consists of large benthic foraminiferal floatstone with a coralline algal wackestone/packstone matrix (Fig. 7C, D). Larger benthic foraminifers are up to 2cm in diameters, thin-shelled, commonly well-preserved (unbroken), and typically horizontally-oriented. The foraminiferal assemblage is dominated by *Spiroclypeus tidoenganensis* with common occurrences of *Cycloclypeus, Eulepidina, Nephrolepidina, Miogypsinoides* and *Amphistegina.* Planktonic foraminifers occur occasionally in LF2.2 lithofacies. Laminar and loose *Mesophyllum*, together with branching *Lithothamnion* are common components.

Interpretation: The foraminiferal assemblage dominated by very large and flat *Spiroclypeus*, *Cycloclypeus* and *Lepidocyclinids*, is typical of oligophotic environments, at depths of 30 m or greater, but could grow comfortably at depths as great as 70 m (Hallock and Glenn, 1986; Noad, 2001). The occurrence of planktonic foraminifera in LF2.2 is consistent with such water depths.

The coralline algal assemblage, dominated by *Mesophyllum* and *Lithothamnion*, is also indicative of relatively low light conditions (e.g., Adey 1979; Bosence 1983; Rosler et al. 2015). The biological composition together with the well preservation state of flat-shaped large benthic foraminifera and the high proportion of micrite matrix strongly suggest that the LF2.2 floatstones were deposited in an oligophotic, low-energy environment.

LF3.1 Coral floatstone with echinoderm-rich wackestone matrix

LF3.1 lithofacies is a scleractinian-dominated floatstone (Fig. 8 A-C, E) consisting of thin branches of unidentified corals or massive fragments of merulinids and pocilloporids. Associated fossils included solitary corals. All are embedded in a wackestone matrix dominated by echinoderm fragments (mainly ophiuroids and some echinoids: Fig. 8D), small pieces of non-articulated coralline algae and occasional benthic foraminifers (mainly broken lepidocyclinids, *Spiroclypeus, Miogypsinoides* and *Amphistegina*). Some rare, well-preserved, flat-shaped lepidocyclinids and *Spiroclypeus* may represent autochtonous biota. The coralline algal assemblage, although poorly preserved, is prominently composed of *Mesophyllum* and *Lithothamnion*. Most of the corals are partially leached and filled with a finely bioclastic micrite (Fig. 8A, C, E) which is identical in nature and in physical continuity with the matrix in which they are embedded (faint ghost fabrics, *sensu* Sanders, 2003). Corals may be also replaced by calcite (Fig. 8B) or may be preserved as molds.

Within the Upper Burman Limestone, LF3.1 has been encountered in four distinct, 5 to 10 m-thick intervals. Brecciated intervals (1 to 3 m-thick) may occur with LF3.1 units (Fig 9). In such breccia, clasts are gravel to pebble-sized (typically 0.5 to 5.0 cm diameter), sub-angular to sub-rounded in shape (Fig. 9A-B) and commonly display deep embayments (Fig 9A). The space

306 between clasts is filled with a lime mud-supported sediment containing various proportions of fine-grained echinoderm fragments. The top of brecciated LF3.1 intervals are characterized by
308 uneven, tightly indurated and brecciated surfaces with angular clasts (WELL-3 1295.5 m on Fig. 9C).

310

Interpretation:

312 The biological assemblage in the matrix of LF3.1 floatstone is dominated by echinoderms and contains low amounts of light-dependent biota, which is not consistent with deposition under
314 euphotic conditions. Benthic foraminifers (mainly broken, flat-shaped lepidocyclinids and *Spiroclypeus*) are extremely scarce and likely derive from oligo-mesophotic environments. In
316 addition, coralline algae are always broken and the assemblage (*Mesophyllum* and *Lithothamnion*) is similar to that of LF1 and LF2. The fragmented nature of corals, red algae and
318 most foraminifers ~~strongly~~ is indicative of displacement. Assemblages of broken benthic foraminifers (lepidocyclinids, *Spiroclypeus*, *Miogypsinoides*) and coralline algae (*Mesophyllum*
320 and *Lithothamnion*) indicate that the transported bioclastic material derives from an area located within the mesophotic domain. It is therefore likely that corals and associated benthic
322 foraminifers and coralline algae, were derived from nearby patches or mounds whose top has reached the mesophotic environment. The importance of coral-dominated carbonate factories in
324 mesophotic settings has been recognized in various Cenozoic carbonate systems, in relation with nutrient-rich and episodically agitated environments (e.g., Morsilli *et al*., 2012; Pomar *et al.,*
326 2014) or with turbid waters (Santodomingo et al., 2015). Under such conditions, corals may develop by enhancing their heterotrophic strategy and thus acting as suspension feeders (e.g.,
328 Anthony, 1999; Morsilli *et al*., 2012). The relative dominance of heterotrophs (echinoderms) and

the lack of *in situ* light-dependent biota (larger benthic foraminifers, coralline algae and zooxanthelate corals) could reflect low light environments (dysphotic to aphotic) due to increased water-depth or water-turbidity. In ancient and modern environments, occurrences of dense ophiuroid populations are regarded as requiring the combination of three conditions (Aronson *et al.*, 1997; Aronson, 2009) : low skeleton-crushing predation, low rates of sediment resuspension, and high flux of particulate organic matter. As a consequence, the development of coral patches in mesophotic settings, coevally with ophiuroid-rich sediment in dysphotic to aphotic area may be interpreted as resulting from high concentrations of suspended particulate organic matter in the water column and associated reduction in light penetration.

In brecciated intervals (Fig. 9A-B), the similarity between the texture and composition of the intraclasts and those of the matrix in which they are embedded, the irregular shape of the clasts which display deep embayments, strongly suggest that brecciation affected a partially lithified lime-mud and therefore occurred early, in marine environments. Similar features of soft deformation and early brecciation have been interpreted by Bouchette et al. (2001) as resulting from water-wave cyclic loading. As a consequence, in spite of prevailing low-energy hydrodynamic conditions which are suggested by the lime-mud-supported nature of LF3.1, episodic high energy events are needed to: (1) break up and removed coral colonies, and (2) trigger sediment brecciation, clast deformation and reworking on the partially-lithified sea-bottom (Bouchette et al., 2001; Seguret et al., 2001). The angular nature of clasts at top of brecciated intervals and the sharp contact with overlying LF1 facies (Fig. 9) suggests that early brecciation processes affected well-lithified limestones (Teillet et al., 2019), and likely occurred during a period of depositional hiatus (hardground).

352 LF3.1 lithofacies therefore is interpreted to have deposited in a low light environment (dysphotic to aphotic), with high concentrations of suspended particulate organic matter, at the vicinity of
354 mesophotic coral patches and subject to episodic high-energy events, such as storms or internal waves, causing sea-floor brecciation.

356

LF3.2 Echinoderm wackestone

358 The LF3.2 lithofacies is a bioclastic wackestone dominated by fragments of echinoderms, including ophiuroid ossicles and echinoids (Fig. 8F). Small-size (< 1 mm) fragments of coralline
360 algae (*Mesophyllum* and *Lithothamnion)* are common. Isolated coral pieces and rare fragments of large benthic foraminifers may be present. LF3.2 facies commonly occurs as layers (0.10 to 1 m-
362 thick) interbedded within LF3.1 coral floatstones.

Interpretation:

364 The similarity in texture and biota between the echinodermal wackestone (LF3.2) and the matrix of the coral floatstone (LF3.1) give evidence that LF3.2 represents a lateral analog of LF3.1,
366 deposited in a dysphotic to aphotic environment. This contention is reinforced by the fact that LF3.2 and LF3.1 form thin (0.10 to 1 m) alternations. Since LF3.1 and LF3.2 essentially differ in
368 their coral abundance, they may reflect a gradient of proximity to mesophotic coral patches.

370 4.2 ***Vertical and lateral changes in lithofacies and related environments***

Vertical changes in lithofacies, related depositional environments and remarkable surfaces are
372 summarized in Fig. 10 and 11 for each well in the cored intervals of the Upper Burman Limestone. All of the lithofacies have been interpreted as being deposited in low to moderate

374 light environments, below the euphotic zone. In the cored sections, the Upper Burman Limestone is subdivided into meter-to-decameter-scale sedimentary units dominated either by LF1, LF2.1
376 and LF2.2 lithofacies (named units FA1 to FA6 in Fig. 10, 11 and 12) or by LF3.1 and LF3.2 lithofacies (units ES1 to ES5: Fig. 10, 11 and 12). Transitions between lithofacies are
378 characterized mainly by gradual changes in biogenic composition. However, the upper part of coral-rich intervals (LF3.1 facies) is typically brecciated and topped by hardground surfaces
380 (Teillet et al., 2019) (Fig. 9C, 10, 11). The correlation framework and the well-to-seismic tie (Fig. 12) revealed that the seismic reflectors roughly follow lithostratigraphic boundaries. For
382 instance, the seismic marker H9B matches with the boundary between a lower, 10 m-thick interval of foraminiferal wackestones (LF2.2) and an upper, massive, interval containing
384 rhodoliths, lepidocyclinids and *Spiroclypeus* (LF1). The stratigraphic correlation between wells reveals a lack of significant lateral change in lithofacies association within the carbonate buildup.
386 Such a stratigraphic architecture is indicative of a lack of significant topographic gradient on top of the buildup. The cored section of the Upper Burman Limestone (Aquitanian-Burdigalian)
388 exhibits five main coral floatstone (LF3) intervals interbedded within foraminiferal-coral algal-dominated intervals (LF1-LF2).

390

4.3 Seismic interpretation

392

The 3D seismic records from~~,~~ the Upper Burman Limestone interval are characterized by a set
394 of flat, continuous, parallel, low to moderate amplitude reflectors (Fig. 13). There is no change in seismic facies or reflector morphology on the edges of the Yadana platform that could be
396 interpreted as suggesting the presence of outer reef rims. The inter-well correlation of seismic

markers is supported by the good lateral continuity of the seismic reflectors within the Upper
398 Burman Limestone (Fig. 13A-C). The lack of significant lateral changes in amplitude, the flat morphology and the parallel pattern of the reflectors are strongly consistent with a layer-caked
400 stratigraphic architecture (low lateral changes in lithofacies and thickness) as suggested by well correlations (Fig. 12). Additionally, seismic reflectors are conform with chronostratigraphic
402 time-lines (Fig. 13 D)

On the seismic profiles, reflectors from the Upper Burman Limestone appear sharply truncated at
404 the northern platform margin (Fig. 13A-C). In addition, the very uneven shape of the reservoir top surface on coherency maps (Fig. 13E) argues for a significant erosion of the Yadana buildup,
406 after the Burdigalian and prior to deposition of the overlying prodelta shales during the Tortonian.

408

5. DISCUSSION

410

5.1 The Yadana buildup: an early Miocene, isolated, oligo-mesophotic carbonate platform

412

The Yadana carbonate platform has been previously interpreted as a shallow-water, reef-rimmed
414 carbonate platform based on seismic facies interpretations (Paumard et al., 2017). Instead, the present environmental interpretations are based on: (1) the nature of the skeletal components and
416 the ecological requirements of the benthic communities from which they have derived, particularly light for autotrophs and food requirements for heterotrophs, (2) rock textures as
418 indicative of water-energy, (3) reconstruction of sedimentary geometries based on well correlations and 2D seismic cross sections analysis.

420 The isolated position of the Yadana carbonate system during the Aquitanian and Burdigalian has been demonstrated by the three-dimensional pattern of seismic data (Paumard et al., 2017). The
422 lateral correlative potential of the lithofacies and their variability in thickness are indicative of a weak topographic gradient, at least in the western part of the buildup. In addition, the carbonate
424 sediments from the Upper Burman Limestone are characterized by the absence of strictly euphotic constituents such as reef dwelling or seagrass-related biota. This suggests that the
426 studied area around wells was not fed by sediments produced by a euphotic carbonate factory. In addition, the lack of lateral changes in the seismic facies and in thickness eastward, as revealed
428 by the seismic data, supports the interpretation of a flat-topped platform for the whole early Miocene Yadana build-up.

430 The layer-caked architecture (=alternating echinodermal-scleractinian and foraminiferal-coralline algal intervals) of the Upper Burman Limestone is indicative of specific environmental
432 conditions (light penetration, nutrient content, water-depth) on the platform top at a given time. In contrast, the vertical changes in lithofacies (Fig. 10, 11, 12) can be interpreted in terms of
434 changing environmental parameters such as nutrient supply, turbidity, water energy and water-depth. The Upper Burman Limestone from the Yadana build-up has recorded three types of
436 carbonate factory that operated on the top of the platform depending on the paleoenvironmental context (1) a scleractinian factory developing under mesophotic conditions in shallow (below
438 fair-weather-wave base?), nutrient-rich waters, (2) an echinodermal factory occupying aphotic to oligophotic area of the shelf coevally with the scleractinian carbonate factory below fair-
440 weather-wave base, and (3) large benthic foraminiferal (LBF)-coralline algal factories prevailing under oligo-mesophotic and oligo-mesotrophic conditions below fair-weather-wave base.

442 *The scleractinian and the echinodermal carbonate factories* (Fig. 14A)

Analysis of the biogenic components and textural features of LF3.1 and LF3.2 lithofacies reveals
444 the existence of two coeval carbonate factories developing on top of the Yadana shelf. During LF3.1 and LF3.2 deposition, the top of the Yadana shelf was mainly located within the disphotic
446 or possibly aphotic zone, and below the fair weather wave base. In such environments, skeletal carbonate production was dominated by echinoderms including a large proportion of ophiuroids.
448 The abundance of ophiuroids in LF3.1 and LF3.2 suggests that prevailing environmental conditions favored the development of suspension-feeders (McKinney and Hageman, 2007). The
450 abundance of coral fragments scattered within echinodermal wackestones (LF3.1), together with broken, mesophotic benthic foraminifers and coralline algae, relies to the existence of a
452 mesophotic scleractinian carbonate factory. However, in-situ coral facies have not been encountered in cores.

454 In modern environments, mesophotic coral communities are known to include both zooxanthellate and azooxanthellate corals and occur in the lower half of the photic zone at depths
456 down to 150 m (e.g., Kahng et al. 2010). In such environments, zooxanthellate corals may exhibit various photo-acclimatization strategies, but can also develop heterotrophic behavior, as
458 suspension feeders, particularly when light significantly decreases with increasing depth or increasing turbidity, or during periods of high nutrient supplies (e.g., Muscatine et al., 1989;
460 Alamaru et al., 2009; Chan et al., 2009; Lesser et al., 2009; Morsilli et al., 2012). In modern (Kahng et al., 2010, and references therein) and ancient low-light environments, corals are
462 known to form low-relief buildups as observed in the late Eocene pro-delta environments from Spain (Morsilli et al., 2012). The strategy of forming mounds is believed to favor the
464 development of suspension feeders since such reliefs promote surrounding turbulent currents capable of carrying picoplanktons and phytoplanktons (Atkinson and Bilger, 1992; Ribes et al.,

466 2003; Pomar and Hallock, 2008; Morsilli et al., 2012;). In the Yadana platform, corals from LF3.1 possibly derive from neighboring patches or mounds whose top is located in mesophotic
468 environment. Since LF3.1 and LF3.2 mostly differ in their coral abundance, they may reflect a gradient of proximity to such a possible mounds. In addition, the lateral changes in thickness
470 (<10m) of coral-rich units, as well as the lateral pinching out of some of these units, may advocate for the existence of localized sources of coral production, scattered on the Yadana
472 shelf, promoting the formation of a mounded, low relief, top of platform morphology (Fig. 14A). The absence of visible positive morphologies on seismic profiles and the relatively flat and
474 continuous expression of seismic reflectors may suggest that: 1) possible mounds have not been preserved, as a result of marine erosion processes, or 2) the height and lateral extension of these
476 mounds are below the vertical and lateral resolution of the seismic (~ 20 m). The latter hypothesis would imply that the difference in elevation between the top of the mound (coral-
478 dominated carbonate factory) which is located within the mesophotic zone and the dysphotic-aphotic platform (echinoderm-dominated carbonate factory) is less than 20 meters. This would
480 be consistent with a steep light gradient within the water column and therefore with high turbidity (Fig. 14D). Such an interpretation is consistent with the size of mesophotic coral
482 mounds (5-20 meters-high) documented in Rupelian (Majella Mountain: Brandano et al., 2018) and Chattian (Salento Peninsula: Tomassetti et al., 2018) ramp systems from the Mediterranean
484 area. Additionally, the coeval development of a scleractinian and an echinodermal carbonate factory may have been favored by increased influxes in suspended organic particulate matter that
486 promoted both suspension feeding behavior of zooxanthelate corals at shallow depths in mesophotic, turbid waters (Anthony, 1999), and the development of ophiuroids in deeper,
488 dysphotic to aphotic setting (Aronson et al., 1997; McKinney & Hageman, 2007). The

occurrence of brecciated intervals within coral-floatstone intervals, together with the common fragmentation of corals, large benthic foraminifera and coralline algae are indicative of episodic high-energy events that could have been generated by storms or internal waves (Morsilli and Pomar, 2012; Pomar et al., 2012). Finally, the pervasive, early dissolution of coral aragonite (faint ghost texture of coral floatstones) is indicative of under-saturated conditions at the sea-bottom which may be related to (1) enhanced organic matter decay coupled with respiration in environments that are enriched in particulate organic-matter (Sanders, 2003), and (2) the influx of cold, CO_2-rich waters from upwelling currents (Feely et al., 2008).

The large benthic foraminiferal-coralline algal carbonate factories (Fig. 14B, C)

Foraminiferal and coralline algal-dominated carbonate sediments (LF1 and LF2.1) are found in 10 to 25 m-thick intervals that are correlatable between the studied wells (Fig. 12). All the identified biological constituents are indicative of mesophotic, oligo-mesotrophic conditions. The lack of euphotic biota within such intervals strongly suggests that there has been no euphotic carbonate factory on the Yadana buildup at that time. The large benthic foraminiferal-coralline algal carbonate factory, that was the source of carbonate sediment of LF1 and LF2.1, is therefore interpreted to have operated on the top of the Yadana shelf, under mesophotic conditions (Fig. 14B). The high micrite content in coralline algal floatstones LF1 advocates for a low energy environment, below wave-action. However, the usual disintegration of branching rhodoliths and the presence of the LBF rudstone LF2.1 argues for a repetitive alternation of low to high energy conditions. Another evidence of high-energy conditions could be the occurrence of thin (< 1 m) beds of well-sorted foraminiferal rudstones (LF2.1) with dominantly non-oriented large benthic foraminifera, interbedded within coralline algal floatstones (Fig. 7B). Such rudstone deposits

likely correspond to the remobilization of the mesophotic carbonate products and redistribution on top of the Yadana shelf during storm or internal wave events.

Flat-shaped, large benthic foraminifers (*Spiroclypeus*, *Cycloclypeus* and *Eulepidina*) which are the dominant biota of LF2.2 are known to characterize oligophotic and oligo-mesotrophic environments (e.g., Buxton and Pedley 1989; Beavington-Penney and Racey 2004; Pomar et al. 2017). The lack of lateral changes in texture, biota and thickness between the wells for LF2.2 intervals, in addition with the high micrite content, are regarded as expressing a deposition on top of a low-energy platform rather than on a ramp system (Fig. 14C).

5.2 Factors controlling the development of mesophotic coral communities on the Yadana platform

As previously discussed, coralline algal and foraminiferal-dominated carbonate factories are linked to oligo-mesophotic settings associated with low-to-moderate turbidity and oligo-mesotrophic waters, while scleractinian and echinodermal carbonate factories developed coevally during periods of suspended particulate nutrient influxes.

Modern mesophotic carbonate buildups have been commonly reported from locations where surface waters are clear and oligotrophic, allowing sufficient light to penetrate to depths of 30–50 m, and where high fluxes of phytoplanktons and zooplanktons are supplied by internal waves (e.g. Hallock, 2001; Pomar et al., 2017). High fluxes of particulate organic matter would also explain the coeval development of echinoderm-dominated deposits in deeper (dysphotic to aphotic) setting. Such an interpretation is supported by various evidences of episodic high-energy events affecting scleractinian-echinoderm facies (LF3.1 and LF3.2) such as the

transportation of mesophotic coral fragments into dysphotic-aphotic environments, and the common occurrence of brecciated intervals (Fig. 9). The Andaman Sea has been extensively studied for the occurrence of high amplitude (> 60 m) internal solitons (e.g., Osborne and Burch, 1980; Hyder et al., 2005; Jantzen et al., 2013). Locally, solitons are related to the occurrence of strong tidal currents in a stratified water column flowing over reliefs inducing abrupt changes in bathymetry, especially, over the seamounts from the Andaman volcanic arc (Hyder et al., 2005). Solitons induce perturbations of the depth of the pycnocline and generate strong currents (Apel et al., 1985). Such phenomena probably also occurred during the early Miocene, at a time when the topographic sill of the Andaman Arc was already formed and may have contributed to enrich shallow-waters in nutrient by mixing with upwelled deeper waters.

An alternative interpretation would be a development of mesophotic coral communities in shallow, turbid waters with high particulate organic matter influx. Scleractinian-dominated bioconstructions that formed in turbid water under significant terrigenous inputs, have been shown to be common in the geological record (Sanders and Baron-Szabo, 2005) and particularly in Cenozoic shallow-water sedimentary systems from southeast Asia (e.g. Wilson, 2005; Novak et al., 2013; Santodomingo et al., 2015, 2016). At present, the Irrawaddy River of Myanmar is one of the muddiest rivers (Licht et al., 2016) inflowing into the northern Andaman Sea and the Gulf of Martaban (Rao et al., 2005). It is the fifth largest river in the world in terms of suspended sediment discharge, known to have been the major source of sediment within the Andaman Sea since the early Miocene (Licht et al., 2016). As a consequence, the Gulf of Martaban is one of the largest perennially turbid zones of the world's oceans. The suspended sediment levels and the area covered by the highly turbid zone have been shown to be strongly governed by the spring-neap tidal cycles (Ramaswamy et al., 2004). South of the Gulf of Martaban, in the Andaman Sea,

around the location of the Yadana field, the nutrients supplied by the Irrawaddy river favor high concentrations of chlorophyll from algae and diatoms in the ocean (Ramaswamy et al., 2004). The late Oligocene and early Miocene paleogeography of the Andaman Sea is quite similar to the modern (Fig. 1A, B). So, the changes over time in sediment and nutrient inputs from the Irrawaddy River have most likely controlled changes in water turbidity and particulate nutrient concentration in the Yadana area. Periods of high terrigenous inputs may have favored the development of suspension feeders and driven the development of a dysphotic to aphotic echinodermal and mesophotic scleractinian carbonate factories. According to this interpretation, the change from a mesophotic platform dominated by large benthic foraminifers and coralline algae to a dysphotic echinodermal platform may have occurred without increasing water-depth (Fig. 14D). As a consequence, in contrast to interpretations by Paumard et al. (2019), our sedimentological results do not support a deepening trend triggered by a rapid relative sea-level rise, toward the top of the platform.

Finally the occurrence of upwelling currents may also have favored the development of mesophotic coral buildups on the Yadana platform. At present, monsoonal activity in the Andaman Sea is known to induce the formation of seasonal upwelling currents, particularly on the margin of Thailand (e.g., Chatterjee et al., 2017). The South Asian Monsoon (SAM), one of the most significant climatic components in the area is known to have occurred as early as the Oligocene-Miocene boundary (Fig. 4B) (Clift et al., 2008; Clift and Vanlaningham, 2010; Betzler et al., 2018). Seasonal upwelling currents, related to monsoonal activity, have been also reported to occur during the Late Miocene in the Andaman Sea (Chakraborty and Ghosh, 2016). The integration of various geochemical and mineralogical proxies by Clift et al. (2008) concluded that monsoon intensification started during the early Miocene (after ~24 Ma) and that

at least 5 cycles of chemical weathering intensity have been recorded during the Aquitanian-
582 Burdigalian interval. Changes in monsoonal activity during the early Miocene that are suggested by such alteration cycles in southeast Asia may have controlled cyclic terrestrial nutrient supplies
584 and upwelling currents in the Andaman sea. As a result, periods of strong upwelling activity and/or high terrestrial nutrient inputs may have favored the development suspension feeders on
586 top of the Yadana platform and the formation of mesophotic coral patches, whereas oligo-mesophotic and oligo-mesotrophic carbonate factories dominated by coralline algae and large
588 benthic foraminifera characterize periods of lower monsoonal intensity.

590

5.3 The significance of oligo-mesophotic carbonate factories in the Cenozoic of southeast
592 Asia

594

The concept of 'tropical carbonate factory', has been extensively used to typify carbonate
596 paleoenvironments in various Cenozoic sub-tropical to tropical areas (Hallock and Glenn, 1986; Schlager, 2000; 2003). Nevertheless, an important number of recent studies in the Mediterranean
598 region (e.g., Morsilli et al. 2012; Pomar et al. 2014, 2017; Brandano et al., 2017) have increasingly identified facies associations and geometries which are significantly different from
600 the standard modern tropical carbonate model based on reef systems and have pointed out the importance of the meso-oligophotic carbonate production by larger benthic foraminifers, red
602 algae, associated to scleractinians. Brandano and Corda (2002) evidenced a lower-middle Miocene tropical ramp in the Central Appenines where the main carbonate production took place
604 in the aphotic and oligophotic zone. Similarly, the role of mesophotic carbonate factories in Oligo-Miocene carbonate systems has been also evidenced in the Perla field (offshore

606 Venezuela, Carribean domain), where most carbonate sediments have been shown to be produced in the oligo-mesophotic domain (Pomar et al., 2015).

608 In tropical, Cenozoic to modern environments from southeast Asia, heterozoan carbonate production has been shown to be significant and sometimes dominant in areas where upwelling 610 and/or terrestrial runoff, high turbidity and cool waters occur (Halfar and Mutti, 2005; Madden and Wilson, 2013; Wilson and Vecsei, 2005). In such environments, heterotrophic and 612 mixotrophic biota are more common than photosynthetic autotrophs (Tomascik et al., 2000; Wilson and Vecsei, 2005). Additionally, most southeast Asian Cenozoic platforms (including 614 isolated platforms) have extensive development of oligophotic facies in moderate to deep photic zone (Wilson and Vecsei, 2005). Under conditions of high nutrient supply and high water 616 turbidity, large scale, isolated and land-attached oligophotic platforms develop in modern environments (Paternoster platform: *Burollet* et al. 1986 ; Spermonde platform: Renema and 618 Troelstra 2001 ; Kalukalukung banks: Roberts and Phipps 1988, Saya de Malha Bank: Hilbertz and Goreau 2002). Cenozoic counterparts have been also described: Berai platform (Saller and 620 Vijaya, 2002); Tonasa platform (Wilson and Bosence, 1996) ; and Melinau platforms (Adams, 1965). In these carbonate systems, the oligophotic carbonate production dominates while a 622 euphotic carbonate production may occur in some shallow water areas (Wilson and Vecsei, 2005), including barrier reefs or shoal rims (e.g. Paternoster and Berai Platforms), or localized 624 patch/pinnacle reefs (e.g., Spermonde shelf). Shallow areas with euphotic carbonate production may be of very reduced extent in some banks or incipiently drowned platforms such as in the 626 Wonosari and Kalukalukuangs platforms (Read, 1985). The present study shows that isolated carbonate systems with exclusive oligo-mesophotic and dysphotic-aphotic carbonate production 628 existed during the early Miocene in Southeast Asia and that “incipiently drowned platform”

conditions persisted throughout the entire early Miocene interval. On the Yadana platform, oligo-
630 mesophotic carbonate production has been persistent during the early Miocene and has been likely promoted by the combination of repeated periods of high terrestrial runoff (Irrawaddy
632 River), upwelling currents related to monsoonal activity and/ or by deep-water mixing controlled by internal waves.

634 Carbonate production dominated by non-framework building biota has been evidenced in Oligo-Miocene, euphotic environments from the Indo-Pacific realm. Probably, the most significant
636 non-framework building euphotic carbonate factory relates to foraminiferal and coralline algal and scleractinian production in sea-grass environments. Isolated carbonate buildups with
638 dominant sea-grass-related carbonate production has been described in the late Oligocene and early Miocene from the Malampaya buildup, Philippines, where changes in trophic states have
640 operated (Fournier et al., 2004). The Malampaya and Yadana isolated systems show a number of similarities, including their predominantly aggrading stratigraphic architecture, the flat-topped
642 morphology of the platform and the relative abundance of coral-rich facies. However, apart from corals, carbonate production in Malampaya is characterized by euphotic, seagrass-inhabiting
644 benthic foraminifera (*Austrotrillina*, soritids, alveolinids, *Neorotalia*, *Miogypsina* and *Miogypsinoides*) whereas in Yadana the large foraminifers (Lepidocyclinids, *Spiroclypeus*) and
646 encrusting coralline algae of oligo-mesophotic affinity are predominant. Additionally, euphotic carbonate production dominated by seagrass dwellers has been also recognized in the Aquitanian
648 and Burdigalian ramps from Nepoui, New Caledonia (Maurizot et al., 2016), and from the Middle-to-Late Miocene Marion Plateau open platform (Conesa *et al.,* 2005) .

650 Accordingly, the study of the Yadana platform provides new insights into tropical carbonate production in southeast Asia during the Cenozoic. Along with the classical euphotic, oligotrophic

652 carbonate factory (Photozoan *sensu* James 1997), dominated by photosynthetic autotrophs and symbiont-bearing organisms including framework-building corals and large benthic foraminifera
654 (e.g., Wilson and Evans, 2002; Saqab and Bourget, 2016), four tropical carbonate factories coexisted on top of southeast Asian isolated buildups during the Miocene: (1) Seagrass-related,
656 euphotic factory, (2) Oligo-mesophotic and oligo-mesotrophic large benthic foraminiferal and coralline algal factory, (3) a scleractinian factory developing under mesophotic conditions, (4) an
658 echinodermal factory in disphotic to aphotic shelves. It also worth mentioning that these four carbonate factories characterize also the Mediterranean Oligocene and lower Miocene carbonate
660 ramps (e.g. Pedley 1998; Pomar et al., 2017; Brandano et al., 2017).

662

CONCLUSION

664

Based on a detailed study of biological and sedimentological features from cores, well-
666 correlations and seismic expression, a revised depositional model of the early Aquitanian to mid Burdigalian carbonates from the Yadana platform is proposed and interpreted in terms of
668 changes in turbidity, hydrodynamic water energy and nutrient availability.

1) The layer-cake architecture inferred from seismic and well-correlations, together with the
670 low lateral changes in lithofacies suggest deposition on top of a flat-topped and open platform throughout the early Miocene interval. Oligo-mesophotic biological associations
672 dominate whereas strictly euphotic constituents are lacking. Three types of carbonate factories operated at the top of the platform, depending on the paleoenvironmental
674 context: (1) a scleractinian factory developing under mesophotic conditions during

periods of particulate nutrient supplies, (2) an echinodermal factory occupying dysphotic to aphotic area of the shelf coevally with the scleractinian carbonate factory, and (3) large benthic foraminiferal-coralline algal factories prevailing under oligo-mesophotic and oligo-mesotrophic conditions.

2) The three fundamental parameters controlling carbonate production on the Yadana platform were: (1) turbidity, (2) nutrient content, and (3) water energy. The dominantly low-energy setting of the oligo-mesophotic deposits suggests that deposition occurred below the fair-weather wave base. Changes from mesophotic to dysphotic-aphotic carbonate factories on the Yadana platform top through time may be related either to a change in water depth, or to a change in water transparency. The usual fragmentation of branching rhodoliths and the occurrence of brecciated intervals within early cemented coral-echinodermal lithofacies are indicative of frequent episodic high energy events such as storms, internal waves and/or cyclones

3) Finally, for the first time in the Oligo-Miocene from southeast Asia, the present case study documents the development history of a strictly oligo-mesophotic isolated carbonate platform with significant development of coral-rich deposits. Changes in monsoonal intensity and terrestrial runoff from the Irrawaddy River are thought to have largely controlled the paleoceanographic history of the Andaman Sea during the early Miocene. Such events were likely responsible for changes in water turbidity and nutrient supplies as well as for the episodic occurrence of upwelling currents. Internal waves may be also regarded as a potential factor controlling both local hydrodynamics and nutrient supplies. Such paleoceanographic conditions, characterized by variable trophic regimes,

promoted development of an incipiently drowned platform, in oligo-mesophotic settings, during the whole early Miocene time interval.

ACKNOWLEDGMENTS

The present study is part of a PhD work (PhD student: Thomas Teillet) funded by TOTAL R&D CARBONATES, Pau, France. TOTAL and partners (CHEVRON, MOGE) are also greatly acknowledged for the database, the technical support and the clearance for publishing the study. This manuscript has also benefited greatly from the detailed and constructive remarks from Prof. Marco Brandano and Dr. Victorien Paumard.

REFERENCES

Adams, C.G., 1970. A reconsideration of the East Indian Letter Classification of the Tertiary. Bull. Brit. Mus. Nat. Hist., Geol. 19, 87–137.

Adams, C.G., 1965. The Foraminifera and stratigraphy of the Melinau Limestone, Sarawak, and its importance in Tertiary correlation. Q. J. Geol. Soc. 121, 283–338.

Adey WH, 1979. Crustose coralline algae as microenvironmental indicators in the Tertiary, in : Gray, J., Boucot, A.J. (Eds.), Historical biogeography, plate tectonics and the changing environment. Oregon State Univ. Press., Corvallis, pp. 459–464.

Alamaru, A., Loya, Y., Brokovich, E., Yam, R., Shemesh, A., 2009. Carbon and nitrogen utilization in two species of Red Sea corals along a depth gradient: Insights from stable isotope analysis of total organic material and lipids. Geochim. Cosmochim. Acta 73, 5333–5342.

Anthony, K.R.N., 1999. Coral suspension feeding on fine particulate matter. J. Exp. Mar Biol. Ecol., 232, 85-106.

Apel, J.R., Holbrook, J.R., Liu, A.K., Tsai, J.J., 1985. The Sulu Sea Internal Soliton Experiment. J. Phys. Oceanogr. 15, 1625-1651.

Aronson, R.B., 2009. Metaphor, inference, and prediction in paleoecology: climate change and the Antarctic bottom fauna, in: Dietl, G.P., Flessa, K.W. (Eds.), Conservation Paleobiology: Using the Past to Manage for the Future, Paleontological Society Short Course. Paleontol. Soc. Pap. 15, pp. 177–194.

728 Aronson, R.B., Blake, D.B., Oji, T., 1997. Retrograde community structure in the late Eocene of Antarctica Retrograde community structure in the late Eocene of Antarctica. Geology 25, 903–
730 906.

Atkinson, M.J., Bilger, R.W., 1992. Effects of water velocity on phosphate uptake in coral reef-
732 flat communities. Limnol. Oceanogr. 37, 273–279.

Bassi, D., 2005. Larger foraminiferal and coralline algal facies in an Upper Eocene storm-
734 influenced, shallow-water carbonate platform (Colli Berici, north-eastern Italy). Palaeogeogr. Palaeoclimatol. Palaeoecol. 226, 17–35.

736 Bassi, D., Hottinger, L., Nebelsick, J.H., 2007. Larger foraminifera from the upper Oligocene of the Venetian area, north-east Italy. Palaeontology 50, 845–868.

738 Beavington-Penney, S.J., Racey, A., 2004. Ecology of extant nummulitids and other larger benthic foraminifera: Applications in palaeoenvironmental analysis. Earth Sc. Rev. 67, 219–265.

740 Berggren, W.A., Kent, D. V., Swisher, C.C., Aubry, M.-P., 1995. A Revised Cenozoic Geochronology and Chronostratigraphy, in: Berggren, W.A., Kent, D.V., Aubry, M.A.,
742 Hardenbol, J. (Eds.), Geochronology, Time Scales, and Global Stratigraphic Correlation. SEPM Spec. Publ. 54, pp. 129-212.

744 Betzler, C., Eberli, G.P., Kroon, D., Wright, J.D., Swart, P.K., Nath, B.N., Alvarez-Zarikian, C.A., Alonso-Garciá, M., Bialik, O.M., Blättler, C.L., Guo, J.A., Haffen, S., Horozal, S., Inoue,
746 M., Jovane, L., Lanci, L., Laya, J.C., Mee, A.L.H., Lüdmann, T., Nakakuni, M., Niino, K., Petruny, L.M., Pratiwi, S.D., Reijmer, J.J.G., Reolid, J., Slagle, A.L., Sloss, C.R., Su, X., Yao,

748 Z., Young, J.R., 2016. The abrupt onset of the modern South Asian Monsoon winds. Scientific Reports 6, 1–10.

750 Betzler, C., Eberli, G.P., Lüdmann, T., Reolid, J., Kroon, D., Reijmer, J.J.G., Swart, P.K., Wright, J., Young, J.R., Alvarez-Zarikian, C., Alonso-García, M., Bialik, O.M., Blättler, C.L.,
752 Guo, J.A., Haffen, S., Horozal, S., Inoue, M., Jovane, L., Lanci, L., Laya, J.C., Hui Mee, A.L., Nakakuni, M., Nath, B.N., Niino, K., Petruny, L.M., Pratiwi, S.D., Slagle, A.L., Sloss, C.R., Su,
754 X., Yao, Z., 2018. Refinement of Miocene sea level and monsoon events from the sedimentary archive of the Maldives (Indian Ocean). Progr. Earth Planet. Sci. 5:5, 1-18.

756 Bosence, D.W.J., 1983. Description and Classification of Rhodoliths (Rhodoids, Rhodolites), in: Peryt, T.M. (Ed.), Coated Grains. Springer, Berlin, Heidelberg, pp. 217–224.

758 Bouchette, F., Séguret, M., Moussine-Pouchkine, A., 2001. Coarse carbonate breccias as a result of water-wave cyclic loading (uppermost Jurassic - South-East Basin, France). Sedimentology
760 48, 767–789.

BouDagher-Fadel, M.K., 2018. Evolution and geological significance of larger benthic
762 foraminifera, second ed. London, UCL press.

BouDagher-Fadel, M.K., 2015. Biostratigraphic and geological significance of planktonic
764 foraminifera, second ed., London, UCL press.

Boudagher-Fadel, M.K., Banner, F.T., 1999. Revision of the stratigraphic significance of the
766 Oligocene-Miocene “Letter-Stages”. Rev. Micropal. 42, 93–97.

Braga, J.C., Aguirre, J., 2004. Coralline algae indicate Pleistocene evolution from deep, open platform to outer barrier reef environments in the northern Great Barrier Reef margin. Coral Reefs 23, 547–558.

Braga, J.C., Bassi, D., Piller, W., 2010. Palaeoenvironmental significance of Oligocene – Miocene coralline red algae – a review, in: Mutti, M., Piller, W., Betzler, C. (Eds.), Carbonate Systems during the Oligocene–Miocene Climatic Transition. Int. Assoc. Sedim., Spec. Publ. 42, pp. 165–182.

Brandano, M., Corda, L., 2002. Nutrients, sea level and tectonics: constrains for the facies architecture of a Miocene carbonate ramp in central Italy. Terra Nova 14, 4, 257–262.

Brandano, M., Cornacchia, I., Tomassetti, L., 2017. Global versus regional influence on the carbonate factories of Oligo-Miocene carbonate platforms in the Mediterranean area. Mar. Petrol. Geol. 87, 188–202.

Brandano, M., Tomassetti, L., Cornacchia, I., 2018. The lower Rupelian cluster reefs of Majella platform, the shallow water record of Eocene to Oligocene transition. Sediment. Geol. 380, 21–30.

Burollet, P.F., Boichard, R., Lambert, B., Villain, J.M., 1986. The Pater Noster Carbonate Platform. Indonesian Petroleum Association, Proceedings 15th Annual Convention, 155– 169.

Buxton, M.W.N., Pedley, H.M., 1989. Short Paper: A standardized model for Tethyan Tertiary carbonate ramps. J. Geol. Soc. London. 146, 746–748.

Chakraborty, P.P., Khan, P.K., 2009. Cenozoic geodynamic evolution of the Andaman-Sumatra subduction margin: Current understanding. Isl. Arc 18, 184–200.

788 Chakraborty, A., Ghosh, A.K., 2016. Ocean upwelling and intense monsoonal activity based on late Miocene diatom assemblages from Neil Island, Andaman and Nicobar Islands, India. Mar. 790 Micropaleontol. 127, 26–41.

Chan, Y.L., Pochon, X., Fisher, M.A., Wagner, D., Concepcion, G.T., Kahng, S.E., Toonen, R.J., 792 Gates, R.D., 2009. Generalist dinoflagellate endosymbionts and host genotype diversity detected from mesophotic (67-100 m depths) coral Leptoseris. BMC Ecol. 9, 1–7.

794 Chatterjee, A., Shankar, D., McCreary, J.P., Vinayachandran, P.N., Mukherjee, A., 2017. Dynamics of Andaman Sea circulation and its role in connecting the equatorial Indian Ocean to 796 the Bay of Bengal. J. Geophys. Res. Ocean. 122, 3200–3218.

Clift, P.D., Hodges, K. V., Heslop, D., Hannigan, R., Van Long, H., Calves, G., 2008. 798 Correlation of Himalayan exhumation rates and Asian monsoon intensity. Nat. Geosci. 1, 875–880.

800 Clift, P.D., Vanlaningham, S., 2010. A climatic trigger for a major Oligo-Miocene unconformity in the Himalayan foreland basin. Tectonics 29, 1–18.

802 Conesa, G., Favre, E., Münch, P., Dalmasso, H., Chaix, C., 2005. Biosedimentary and paleoenvironmental evolution of the southern Marion platform from the Middle to Late Miocene 804 (Northeast Australia, ODP LEG 194, sites 1196 and 1199), in: Anselmetti, F.S., Isern, A.R., Blum, P., Betzler, C. (Eds.), Proceedings of the Ocean Drilling Program, Scientific Results. 806 College Station, TX (Ocean Drilling Program) 194, pp.1-38.

Curray, J.R., 2005. Tectonics and history of the Andaman Sea region. J. Asian Earth Sci. 25, 808 187–232.

Feely, R.A., Sabine, C.L., Hernandez-Ayon, J.M., Ianson, D., Hales, B., 2008. Evidence for upwelling of corrosive "acidified" water onto the continental shelf. Science 320, 5882, 1490–1492.

Fournier, F., Montaggioni, L., Borgomano, J., 2004. Paleoenvironments and high-frequency cyclicity from Cenozoic South-East Asian shallow-water carbonates: A case study from the Oligo-Miocene buildups of Malampaya (Offshore Palawan, Philippines). Mar. Petrol. Geol. 21, 1–21.

Freiwald, A., Henrich, R., 1994. Reefal coralline algal build-ups within the Arctic Circle: morphology and sedimentary dynamics under extreme environmental seasonality. Sedimentology 41, 963–984.

Gradstein, F., Ogg, J., Schmitz, M., Ogg, G., 2012. The Geologic Time Scale 2012, Elsevier.

Halfar, J., Mutti, M., 2005. Global dominance of coralline red-algal facies: A response to Miocene oceanographic events. Geology 33, 481–484.

Hallock, P., Glenn, E.C., 1986. Larger Foraminifera: A Tool for Paleoenvironmental Analysis of Cenozoic Carbonate Depositional Facies. Palaios 1, 55–64.

Hallock, P., Schlager, W., 1986. Nutrient excess and the demise of coral reefs and carbonate platforms. Palaios 1, 389-398.

Hallock, P., Pomar, L., 2008. Cenozoic evolution of larger benthic foraminifers: Paleoceanographic evidence for changing habitats. Proc. 11th Internat. Coral Reef Symp., Ft. Lauderdale, Florida, pp. 16–20.

Hilbertz, W., Goreau, T., 2002. Saya de Malha Expedition Report, Lighthouse Foundation.

830 Holbourn, A., Kuhnt, W., Schulz, M., Erlenkeuser, H., 2005. Impacts of orbital forcing and atmospheric carbon dioxide on Miocene ice-sheet expansion. Nature 438, 483–487.

832 Hyder, P., Jeans, D.R.G., Cauquil, E., Nerzic, R., 2005. Observations and predictability of internal solitons in the northern Andaman Sea. Appl. Ocean Res. 27, 1–11.

834 James, N.P., 1997. The cool-water carbonate depositional realm, in: James, N.P., Clarke, J. (Eds.), Cool-water Carbonates. SEPM Spec. Publ. 56, pp. 1-20.

836 Jantzen, C., Schmidt, G.M., Wild, C., Roder, C., Khokiattiwong, S., Richter, C., 2013. Benthic reef primary production in response to large amplitude internal waves at the Similan Islands 838 (Andaman Sea, Thailand). PLoS One 8, 1–16.

Kahng, S.E., Garcia-Sais, J.R., Spalding, H.L., Brokovich, E., Wagner, D., Weil, E., Hinderstein, 840 L., Toonen, R.J., 2010. Community ecology of mesophotic coral reef ecosystems. Coral Reefs 29, 255–275.

842 Lesser, M.P., Slattery, M., Leichter, J.J., 2009. Ecology of mesophotic coral reefs. J. Exp. Mar. Bio. Ecol. 375, 1–8.

844 Licht, A., Reisberg, L., France-Lanord, C., Naing Soe, A., Jaeger, J.J., 2016. Cenozoic evolution of the central Myanmar drainage system: Insights from sediment provenance in the Minbu Sub-846 Basin. Basin Res. 28, 237–251.

Madden, R.H.C., Wilson, M.E.J., 2013. Diagenesis of a SE Asian Cenozoic carbonate platform 848 margin and its adjacent basinal deposits. Sediment. Geol. 286–287, 20–38.

Maurizot, P., Cabioch, G., Fournier, F., Leonide, P., Sebih, S., Rouillard, P., Montaggioni, L., 850 Collot, J., Martin-Garin, B., Chaproniere, G., Braga, J.C., Sevin, B., 2016. Post-obduction

carbonate system development in New Caledonia (Népoui, Lower Miocene). Sediment. Geol. 331, 42–62.

McKinney, F.K., Hageman, S.J., 2007. Crossing the Ecological Devide: Paleozoic to Modern Marine Ecosystems in the Adriatic Sea. The Sedimentary Record 5, 4-8.

Miller, K.G., Kominz, M.A., Browning, J. V., Wright, J.D., Mountain, G.S., Katz, M.E., Sugarman, P.J., Cramer, B.S., Christie-Blick, N., Pekar, S.F., 2005. The phanerozoic record of global sea-level change. Science 310, 1293–1298.

Morley, C.K., 2017. Chapter 4 Cenozoic rifting, passive margin development and strike-slip faulting in the Andaman Sea: a discussion of established v. new tectonic models, in: Bandopadhyay, P.C., Carter, A. (Eds.), The Andaman–Nicobar Accretionary Ridge: Geology, Tectonics and Hazards. Geol. Soc. London, Mem. 47, pp. 27–50.

Morsilli, M., Bosellini, F.R., Pomar, L., Hallock, P., Aurell, M., Papazzoni, C.A., 2012. Mesophotic coral buildups in a prodelta setting (Late Eocene, southern Pyrenees, Spain): A mixed carbonate-siliciclastic system. Sedimentology 59, 766–794.

Morsilli, M., Pomar, L., 2012. Internal waves vs. surface storm waves: A review on the origin of hummocky cross-stratification. Terra Nova 24, 273–282.

Muscatine, L., Falkowski, P.G., Dubinsky, Z., Cook, P.A., McCloskey, L.R., 1989. The Effect of External Nutrient Resources on the Population Dynamics of Zooxanthellae in a Reef Coral. Proc. R. Soc. B Biol. Sci. 236, 311–324.

870 Noad, J., 2001. The Gomantong Limestone of eastern Borneo: A sedimentological comparison with the near-contemporaneous Luconia Province. Palaeogeogr. Palaeoclimatol. Palaeoecol. 175,
872 273–302.

Osborne, A.R., Burch, T.L., 1980. Internal Solitons in the Andaman Sea. Science 208, 4443,
874 451–460.

Novak, V., Santodomingo, N., Rösler, A., Di Martino, E., Braga, J.-C., Taylor, P.D., Johnson,
876 K.G., Renema, W., 2013. Environmental reconstruction of a late Burdigalian (Miocene) patch reef in deltaic deposits (East Kalimantan, Indonesia). Palaeogeogr. Palaeoclimatol. Palaeoecol.,
878 374, 110–122.

Paumard, V., Zuckmeyer, E., Boichard, R., Jorry, S.J., Bourget, J., Borgomano, J., Maurin, T.,
880 Ferry, J.N., 2017. Evolution of Late Oligocene - Early Miocene attached and isolated carbonate platforms in a volcanic ridge context (Maldives type), Yadana field, offshore Myanmar. Mar.
882 Petrol. Geol. 81, 361–387.

Pedley, H.M., 1998. A review of sediment distributions and processes in Oligo-Miocene ramps
884 of southern Italy and Malta (Mediterranean divide). Geol. Soc., London. Spec. Publ. 149, 163–179.

886 Pomar, L., 2001. Types of carbonate platforms: A genetic approach. Basin Res. 13, 313–334.

Pomar, L., Hallock, P., 2008. Carbonate factories: A conundrum in sedimentary geology. Earth
888 Sci. Rev. 87, 134–169.

Pomar, L., Morsilli, M., Hallock, P., Badenas, B., 2012. Internal waves, an under-explored
890 source of turbulence events in the sedimentary record. Earth Sci. Rev. 111, 56–81.

Pomar, L., Mateu-Vicens, G., Morsilli, M., Brandano, M., 2014. Carbonate ramp evolution during the Late Oligocene (Chattian), Salento Peninsula, southern Italy. Palaeogeogr. Palaeoclimatol. Palaeoecol. 404, 109–132.

Pomar, L., Martinez, W., Espino, D., Ott, V.C. De, Benkovics, L., 2015. Oligocene-Miocene Carbonates of the Perla Field, Offshore Venezuela: Depositional Model and Facies Architecture, in: Bartolini, C., Mann, P. (Eds.), Petroleum Geology and Potential of the Colombian Caribbean Margin. AAPG Mem. 108, pp. 647-673.

Pomar, L., Baceta, J.I., Hallock, P., Mateu-Vicens, G., Basso, D., 2017. Reef building and carbonate production modes in the west-central Tethys during the Cenozoic. Mar. Petrol. Geol. 83, 261–304.

Pyle, R.L., Boland, R., Bolick, H., Bowen, B.W., Bradley, C.J., Kane, C., Kosaki, R.K., Langston, R., Longenecker, K., Montgomery, A., Parrish, F.A., Popp, B.N., Rooney, J., Smith, C.M., Wagner, D., Spalding, H.L., 2016. A comprehensive investigation of mesophotic coral ecosystems in the Hawaiian Archipelago. PeerJ 4, e2475

Racey, A. and Ridd, M.F., 2015. Petroleum geology of the Moattama Region, Myanmar, in: Racey, A and Ridd, M.F. (Eds.), Petroleum Geology of Myanmar. Geol. Soc. Memoir 45, pp. 63-81.

Rahmani, A., Vaziri-Moghaddam, H., Taheri, A., Ghabeishavi, A., 2009. A model for the paleoenvironmental distribution of larger foraminifera of Oligocene-Miocene carbonate rocks at Khaviz Anticline, Zagros Basin, SW Iran. Hist. Biol. 21, 215–227.

Ramaswamy, V., Rao, P.S., Rao, K.H., Thwin, S., Rao, N.S., Raiker, V., 2004. Tidal influence
912 on suspended sediment distribution and dispersal in the northern Andaman Sea and Gulf of Martaban. Mar. Geol. 208, 33–42.

914 Rao, P.S., Ramaswamy, V., Thwin, S., 2005. Sediment texture, distribution and transport on the Ayeyarwady continental shelf, Andaman Sea. Mar. Geol. 216, 239–247.

916 Read, J.F., 1985. Carbonate Platforms Facies Model. Am. Assoc. Pet. Geol. Bull. 69, 1-21.

Renema, W., Troelstra, S.R., 2001. Larger foraminifera distribution on a mesotrophic carbonate
918 shelf in SW Sulawesi (Indonesia). Palaeogeogr. Palaeoclimatol. Palaeoecol. 175, 125–146.

Ribes, M., Coma, R., Atkinson, M.J., Kinzie, R.A., 2003. Particle removal by coral reef
920 communities: Picoplankton is a major source of nitrogen. Mar. Ecol. Prog. Ser. 257, 13–23.

Roberts, H., Phipps, C.V., 1988. Proposed oceanographic controls on modern Indonesian reefs :
922 A turn-off/turn-on mechanism in a monsoonal setting. Proc. 6th Int. Coral Reef Symp. South Sulawesi, 3, pp.529-534.

924 Rösler, A., Pretkovi, V., Novak, V., Renema, W., Braga, J.C., 2015. Coralline Algae From the Miocene Mahakam Delta (East Kalimantan, Southeast Asia). Palaios 30, 83–93.

926 Saller, A.H., Vijaya, S., 2002. Depositional and diagenetic history of the Kerendan carbonate platform, Oligocene, Central Kalimantan, Indonesia. J. Petrol. Geol. 25, 123–150.

928 Sanders, D., 2003. Syndepositional dissolution of calcium carbonate in neritic carbonate environments: Geological recognition, processes, potential significance. J. African Earth Sci., 36,
930 99-134.

Sanders, D., Baron-Szabo, R.C., 2005. Scleractinian assemblages under sediment input: their characteristics and relation to the nutrient input concept. Paleogeogr. Paleoclim. Paleoecol., 216, 139-181.

Santodomingo, N., Novak, V., Pretkovic, V, Marshall, N., Di Martino, E., Lo Giudice Capelli, E., Rösler, A., Reich, S., Braga, J.-C., Renema, W., Johnson, K.G., 2015. A diverse patch reef from turbid habitats in the Middle Miocene (East Kalimantan, Indonesia). Palaios, 30, 128–149.

Santodomingo, N., Renema, W., Johnson, K.G., 2016. Understanding the murky history of the Coral Triangle: Miocene corals and reef habitats in East Kalimantan (Indonesia). Coral Reefs, 35, 765-781.

Saqab, M.M., Bourget, J., 2016. Seismic geomorphology and evolution of early-mid Miocene isolated carbonate build-ups in the Timor Sea, North West Shelf of Australia. Mar. Geol. 379, 224–245.

Schlager, W., 2000. Sedimentation rates and growth potential of tropical, cool-water and mud-mound carbonate factories,. Geol. Soc. Spec. Publ. 178, 217–227.

Schlager, W., 2003. Benthic carbonate factories of the Phanerozoic. Int. J. Earth Sci. 92, 445–464.

Seguret, M., Moussine-Pouchkine, A., Raja Gabaglia, G., Bouchette, F., 2001. Storm deposits and storm-generated coarse carbonate breccias on a pelagic outer shelf (South-East Basin, France). Sedimentology 48, 231–254.

Teillet, T., Fournier, F., Gisquet, F., Montaggioni, L. F., Borgomano, J., Villeneuve, Q., Hong, F., 2019. Diagenetic history and porosity evolution of an Early Miocene carbonate buildup

952 (Upper Burman Limestone), Yadana gas field, offshore Myanmar. Mar. Petrol. Geol. 109, 589–606.

954 Tomascik, T., Mah, A.J., Nontji, A., Moosa, M.K., 2000. The Ecology of the Indonesian Seas. Part I. The Ecology of Indonesia Series, Volume VII, Periplus Editions.

956 Tomassetti, L., Petracchini, L., Brandano, M., Trippetta, F., Tomassi, A., 2018. Modeling lateral facies heterogeneity of an upper Oligocene carbonate ramp (Salento, southern Italy). Mar. Petrol. 958 Geol. 96, 254–270.

Wade, B.S., Pearson, P.N., Berggren, W.A., Pälike, H., 2011. Review and revision of Cenozoic 960 tropical planktonic foraminiferal biostratigraphy and calibration to the geomagnetic polarity and astronomical time scale. Earth Sci. Rev. 104, 111–142.

962 Wilson, M.E.J., 2002. Cenozoic carbonates in Southeast Asia: Implications for equatorial carbonate development. Sediment. Geol. 147, 295–428.

964 Wilson, M.E.J., 2005. Development of equatorial delta-front patch reefs during the Neogene, Borneo. J. Sediment. Res. 75, 114–133.

966 Wilson, M.E.J., 2008. Global and regional influences on equatorial shallow-marine carbonates during the Cenozoic. Palaeogeogr. Palaeoclimatol. Palaeoecol. 265, 262–274.

968 Wilson, M.E.J., Bosence, D.W.J., 1996. The Tertiary evolution of South Sulawesi: a record in redeposited carbonates of the Tonasa Limestone Formation, in: Hall, R., Blundle, D. (Eds.), 970 Tectonic Evolution of Southeast Asia. Geol. Soc. London, Spec. Publ. 106, pp. 365–389.

Wilson, M.E.J., Evans, M.J., 2002. Sedimentology and diagenesis of Tertiary carbonates on the Mangkalihat Peninsula, Borneo: Implications for subsurface reservoir quality. Mar. Petrol. Geol. 19, 873–900.

Wilson, M.E.J., Vecsei, A., 2005. The apparent paradox of abundant foramol facies in low latitudes: Their environmental significance and effect on platform development. Earth Sci. Rev. 69, 133–168.

Wilson, M.E.J., Hall, R., 2010. Tectonic influences on SE Asian carbonate systems and their reservoir development, in: Morgan, W.A., George, A.D., Harris, P.M., Kupecz, J.A., Sarg, J.F. (Eds.), Cenozoic Carbonate Systems of Australasia. SEPM Spec. Publ. 95, pp. 13–40.

Figure and table caption

Fig. 1. (A) Location map of the Yadana field and tectonic setting of the Andaman Sea (after Curray 2005); (B) and (C) Paleogeography of the Andaman Sea and environmental setting of the Yadana platform during the early Miocene (B) and late Oligocene (B) (modified from Licht *et al.,* 2016 ; Morley, 2017).

Fig. 2. Morphological and geophysical frame of the Yadana field (A) Depth map of the top reservoir surface interpreted from 2D seismic data showing the Yadana High, the M5 and the Moattama basins. The red square represents the 3D seismic survey of the Yadana Field and the red line refers to the seismic profile (Fig. 2C). (B) 3D Seismic survey of the Yadana Field, depth map of the top reservoir surface and well location. (C) Interpreted regional 2D seismic profile through the Yadana High (with location of projected WELL-1, WELL-2, WELL-3, WELL-4). (D) Depth map of horizon H10B (early Aquitanian), well location and outlines of the Yadana platform during the early Aquitanian (base of cored interval). (E) Depth map of horizon H9B (N6 zone: Burdigalian), well location and outlines of the Yadana platform during the Burdigalian.

Fig. 3. Seismic architecture and stratigraphy of the Yadana carbonate platform: (A) Interpreted 3D seismic profile (location on the Fig. 2.B.) of the Yadana Field passing across the wells WELL-4 and WELL-2. The lithostratigraphic units and the gas water contact (yellow dotted line) are showed (B). Lithostratigraphic column of the Yadana platform, name and age of the sedimentary units.

1006 **Fig. 4.** Chronostratigraphic framework of the Yadana carbonate platform (synthesis of the four studied wells): (A) based on planktonic and large benthic foraminifera from cores and side wall
1008 samples. (B) Chronostratigraphic framework of the Yadana field, eustacy (Miller *et al.,* 2005) and global climatic events: (1) late Oligocene-early Miocene warming and Mi-1 glaciation
1010 (Holbourn *et al.,* 2005), (2) intensity of Proto-monsoon and South Asian Monsoon (Betzler *et al.,* 2016).

1012

Fig. 5. Microphotographs of key large benthic foraminifera of the UBL formation: (A) WELL-2
1014 1354, 95 mCD: *Miogypsinella ubaghsi* (Tan Sin Hok, 1936). (B) WELL-3 1350, 24 mCD: *Miogypsina intermedia* (Drooger, 1952); (C) WELL-1 1254, 3 mCD: *Miogypsinoides*
1016 *bantamensis* (Tan Sin Hok, 1936). (D) WELL-2 1329, 22 mCD: *Globigerinoides primordius* (Blow and Banner, 1962), E) WELL-1 1243, 88 mCD: a - *Spiroclypeus tidoenganensis* (Van
1018 der Vlerk, 1925); b – *Miogypsina subiensis* (BouDagher-Fadel and Price, 2013). (F) WELL-1 1259, 50 mCD: *L. (Nephrolepidina) sumatrensis* (Brady, 1875)

1020

1022 **Fig. 6.** Microphotographs (A – F) and core photograph (G) of coralline algal floatstones and rudstones (LF1): (A) WELL-3 1321.97 m: Coralline algal rudstone (LF1). Encrusting
1024 (rhodolith) and warty forms, possible *Lithothamnion* **(Lith)** with small conceptacles. (B) WELL-1 1251.25 m: Coralline algal floatstone (LF1). Branching *Lithothamnion* **(Lith)** with flat (and
1026 filled) conceptacles. *L. ramossissimum* type. (C) WELL-3 1323.40 m: Coralline algal floatstone (LF1) with a foraminiferal-red algal grainstone matrix. Encrusting and branching *Lithothamnion*

1028 **(Lith)** with flat conceptacles, *L. ramossissimum* type, (D) WELL-2 1262.68 m: Coralline algal floatstone (LF1). Abundant protuberant crusts of *Sporolithon* **(Sporo)**, (E) WELL-3 1334.48 m:
1030 Coralline algal floatstone (LF1) with a foraminiferal grainstone matrix (LF1). Branching and encrusting forms of coralline algae **(RA)** associated with *Miogypsinoides* **(Miog)**. (F) WELL-3
1032 1340.90 m: Coralline algal with large benthic foraminiferal floatstone-wackestone (LF2.2). Laminar, loose *Mesophyllum* **(Meso)**. (G) WELL-2 1345 m: Core picture of rhodolothic
1034 rudstone. Rudstone. Black bar length = 7 mm. (G)

1036 **Fig. 7.** Microphotographs of foraminiferal rudstones (LF2.1) and foraminiferal floatstone (LF2.2): (A) WELL-1 1319.49 m: Large benthic foraminiferal rudstone (LF2.1) with broken
1038 specimens of *Spiroclypeus* and *Lepidocyclinids (Lepidocyclina spp).* Space between bioclasts is filled by calcitic cements. (B) WELL-2 1291.8 m: Oriented core sample of lithofacies LF2.1.
1040 (C) WELL-1 1270.70 m: large benthic foraminiferal floatstone (LF2.2) with flat *Spiroclypeus* **(Spiro)**, laminar coralline algae **(RA)** and small pieces of corals **(Coral)**. (D) WELL-3 1344.98
1042 m: Large benthic foraminiferal floatstone (LF2.2) with flat-shaped *Cycloclypeus* **(Cyclo)**, *Spiroclypeus* **(Spiro)** and laminar coralline algae **(RA)**.

1044

Fig. 8. Microphotographs of coral floatstones (LF3.1) and echinodermal wackestones (LF3.2):
1046 (A) WELL-1294.98 m: leached corals **(Coral)** filled with lime mud (faint ghost texture) set in fine bioclastic wackestone matrix with rare flat large benthic foraminifers **(LBF)** and
1048 echinoderms **(Echi)**. (B) WELL-2 1361.42 m: Cemented coral fragment in a wackestone-packestone bioclastic matrix dominated by echinoderm fragments (C) WELL-1 1294.7 m:
1050 leached coral in echinodermal wackestone. (D) WELL-4 1258.03 m: Section of ophiuroids

within the matrix of a coral floatstone LF3.1 **(1)**. (E) WELL-3 1311.84 m: Dissolved coral (LF3.1) filled with fine bioclastic micritic matrix (F) WELL-4 1326.22 m: Bioclastic packestone-wackestone with fragments of echinoderms **(Echi)** (LF3.2).

Fig.9. Core photographs of brecciated LF3 intervals: (A) WELL-1 1256.6 m: brecciated coral floatstone with irregular-shaped clasts showing deep embayments. (B) WELL-4 1258.03 m: microphotograph showing a brecciated echinodermal wackestone (LF3.2). The sediment between clasts consists of lime mud. Clasts display irregular shapes with smooth edges which suggest that brecciation affected a relatively soft, partially lithified sediment; (C) WELL-3 1308.05 m: core photograph of a hardground surface, at the top of a carbonate breccia composed of poorly displaced, tight elements of coral-rich and echinodermal floatstone (LF3). The hardground is sharply overlain by highly microporous, coralline algal-foraminiferal floatstone (diagenetic facies: G-DF1A). The space between clasts is filled by the overlying microporous sediment.

Fig. 10. Description of cores in terms of textures, bio-constituents, large benthic foraminiferal taxa, and morphologies, coralline algal morphologies and environmental interpretations: WELL-2 (A) and WELL-3 (B).

Fig. 11. . Description of cores in terms of textures, bio-constituents, large benthic foraminiferal taxa, and morphologies, coralline algal morphologies and environmental interpretations: WELL-1 (A) and WELL-4 (B).

Fig. 12. Well-correlations and stratigraphic architecture of the Yadana platform, based on large benthic foraminiferal biostratigraphy, well-to seismic tie (vertical resolution ~20m) and correlation of lithofacies associations. Names of depositional units refer to coralline algal-foraminiferal carbonate factories (FA) and Echinodermal / Scleractinian carbonate factories (ES).

Fig. 13. Seismic geometries of the Yadana platform. The location of seismic profiles are indicated on Fig. 13E (red lines). (A) SE-NW-oriented, crossing through wells WELL-3 and WELL-4 and illustrating the main reflectors within the Upper Burman Limestone. (B) E-W-orientated profile, (C) N-S-oriented profile, and (D) W-E-oriented profile, through WELL-4 and WELL-2 (WELLE-1: projected). The gas water contact is identifiable on this line by a nearly horizontal reflector cross-cutting time-lines. (E) Coherency map of the top reservoir surface.

Fig. 14. Depositional models for the flat-topped, oligo-mesophotic Yadana platform during the early Miocene (cored interval), for distinct paleooceanographic settings: (A) Mesophotic scleractinian mounds developing on top of a platform with dominant echinodermal carbonate production in dysphotic to aphotic conditions; the development of coral buildups results from significant supplies in particulate organic matter from various potential sources (upwelling currents, internal waves or terrigenous runoff); (B) Mesophotic, coralline algal-foraminiferal carbonate production prevailing on the platform top, under oligotrophic to mesotrophic conditions; (C) Oligophotic, large benthic foraminiferal carbonate production under oligotrophic to mesotrophic conditions; (D) Paleowater-depth estimates for the distinct carbonate factories. Two hypotheses of water turbidity are considered for the mesophotic coral mounds. The light-

intensity zonation with depth is based on the proportion of surface light for different extinction coefficients of light (modified from Morsilli et al. 2012). Lower limit of the euphotic, mesophotic and oligophotic zones depends on water transparency. Curves of light penetration for different extinction coefficients of light are based on Hallock and Schlager (1986); Kahng et al., (2010).

Table 1. Lithofacies classification and paleoenvironmental interpretations of the UBL formation, based on the main skeletal components and sedimentological attributes.

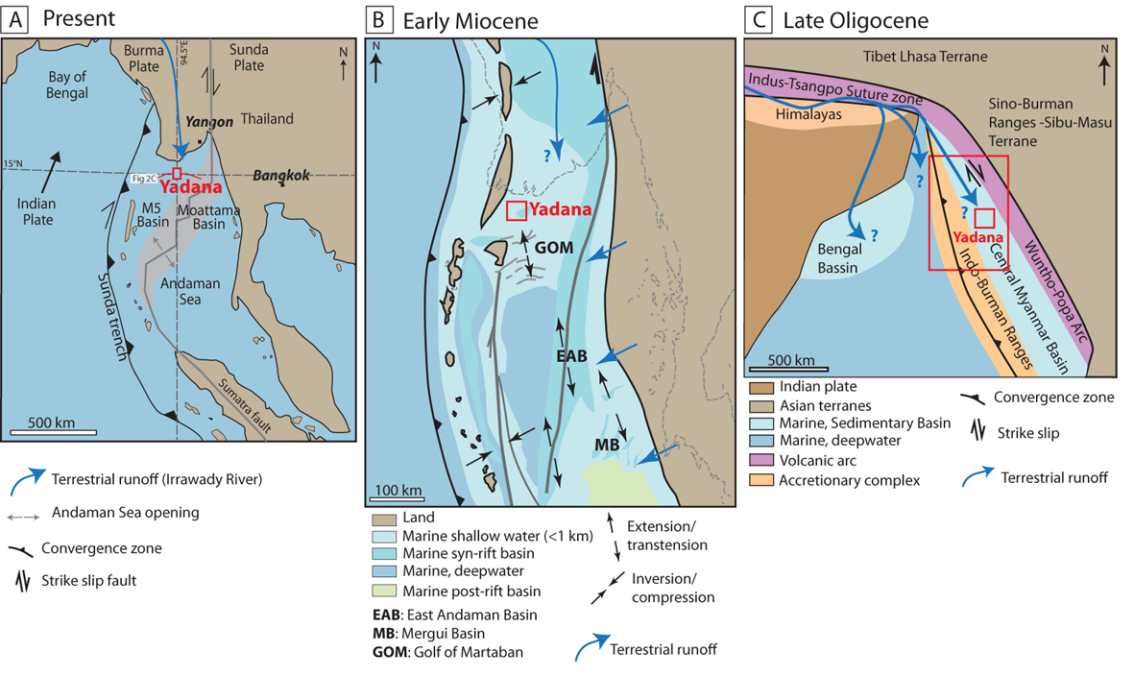
A Present
Burma Plate
94.5°E
Sunda Plate
N
Bay of Bengal
Yangon
Thailand
15°N
Fig 2C
Yadana
Bangkok
Indian Plate
M5 Basin
Moattama Basin
Andaman Sea
Sunda Trench
Sumatra fault
500 km
Terrestrial runoff (Irrawady River)
Andaman Sea opening
Convergence zone
Strike slip fault
B Early Miocene
N
Yadana
GOM
EAB
MB
100 km
Land
Marine shallow water (<1 km)
Marine syn-rift basin
Marine, deepwater
Marine post-rift basin
EAB: East Andaman Basin
MB: Mergui Basin
GOM: Golf of Martaban
Extension/ transtension
Inversion/ compression
Terrestrial runoff
C Late Oligocene
Tibet Lhasa Terrane
N
Indus-Tsangpo Suture zone
Himalayas
Sino-Burman Ranges -Sibu-Masu Terrane
Bengal Bassin
Yadana
Indo-Burman Ranges
Central Myanmar Basin
Wuntho-Popa Arc
500 km
Indian plate
Asian terranes
Marine, Sedimentary Basin
Marine, deepwater
Volcanic arc
Accretionary complex
Convergence zone
Strike slip
Terrestrial runoff

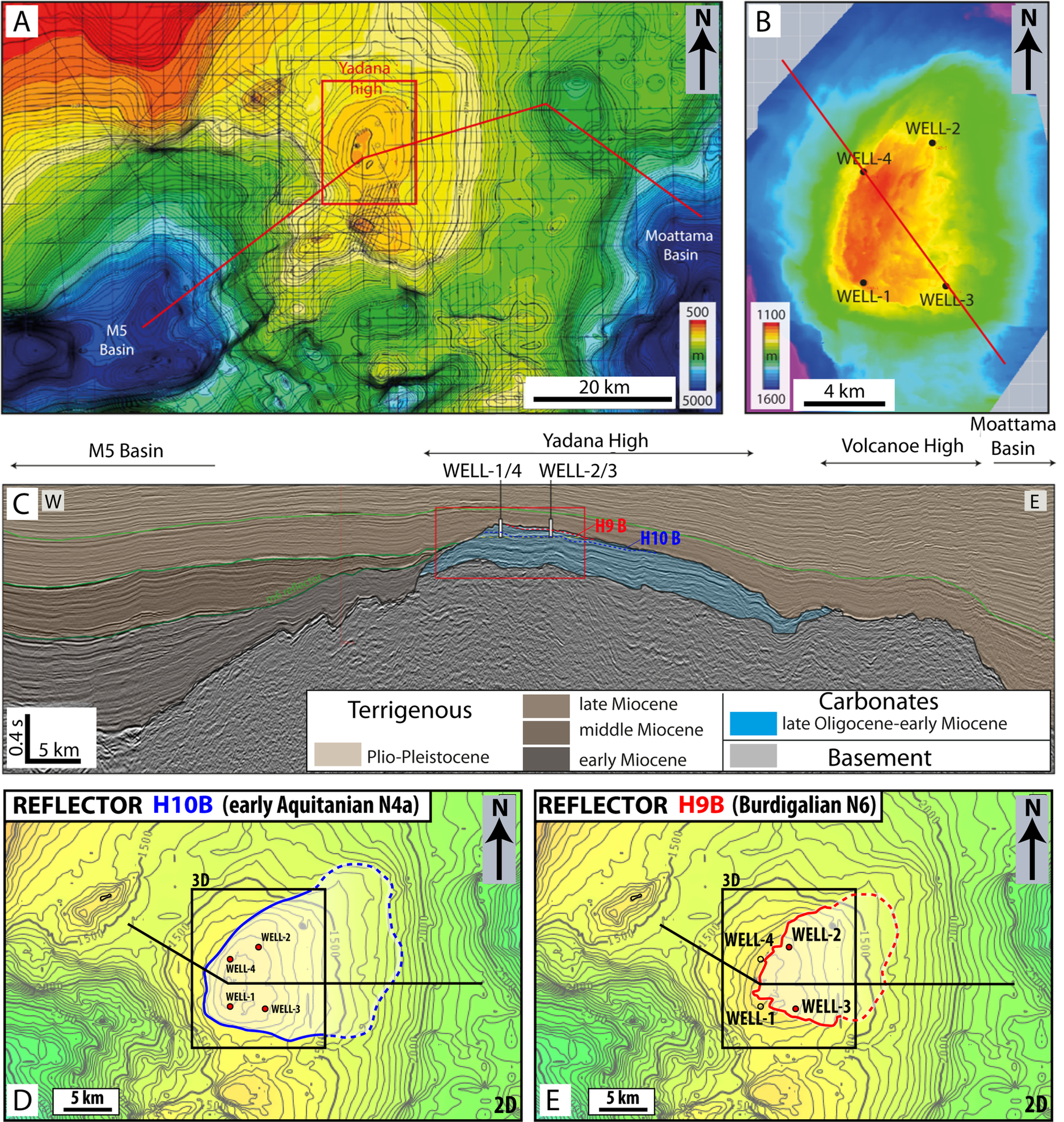
A
N
Yadana high
Moattama Basin
M5 Basin
500
m
5000
20 km
B
N
WELL-2
WELL-4
WELL-1
WELL-3
1100
m
1600
4 km
M5 Basin
Yadana High
Volcanoe High
Moattama Basin
WELL-1/4
WELL-2/3
C
W
E
H9 B
H10 B
0.4 s
5 km
Terrigenous
Plio-Pleistocene
late Miocene
middle Miocene
early Miocene
Carbonates
late Oligocene-early Miocene
Basement
REFLECTOR H10B (early Aquitanian N4a)
N
3D
WELL-2
WELL-4
WELL-1
WELL-3
D
5 km
2D
REFLECTOR H9B (Burdigalian N6)
N
3D
WELL-4
WELL-2
WELL-1
WELL-3
E
5 km
2D

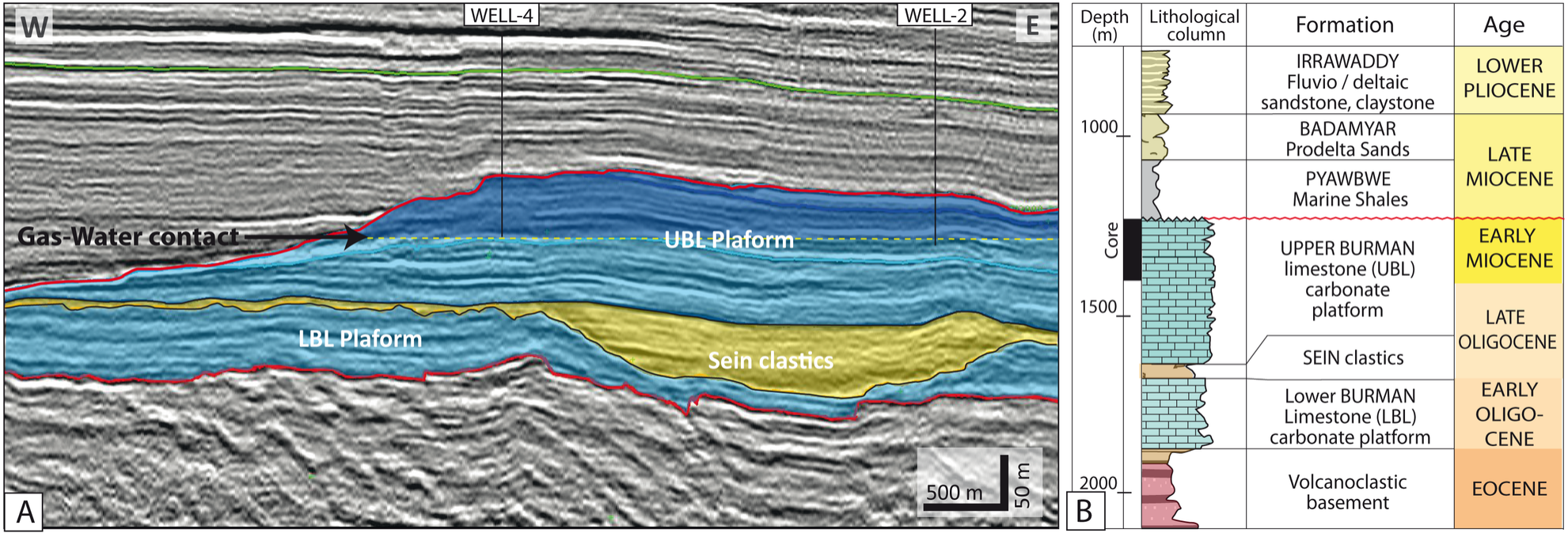
W
WELL-4
WELL-2
E
Gas-Water contact
UBL Plaform
LBL Plaform
Sein clastics
500 m
50 m
A
Depth (m)
Lithological column
Formation
Age
IRRAWADDY
Fluvio / deltaic sandstone, claystone
LOWER PLIOCENE
1000
BADAMYAR
Prodelta Sands
LATE MIOCENE
PYAWBWE
Marine Shales
Core
UPPER BURMAN
limestone (UBL)
carbonate platform
EARLY MIOCENE
1500
LATE OLIGOCENE
SEIN clastics
Lower BURMAN
Limestone (LBL)
carbonate platform
EARLY OLIGO-CENE
2000
Volcanoclastic basement
EOCENE
B

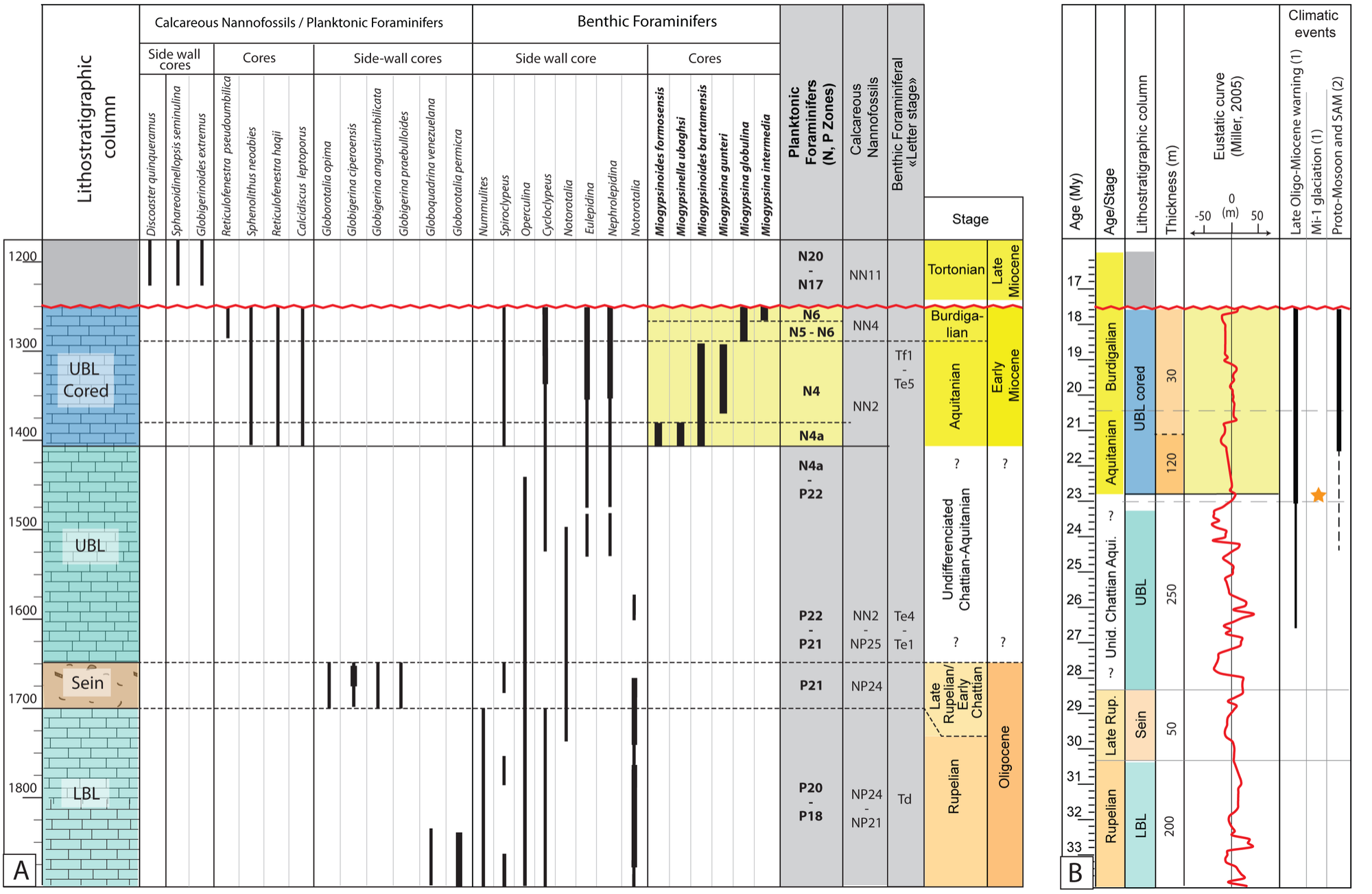
Lithostratigraphic column
Calcareous Nannofossils / Planktonic Foraminifers
Side wall cores
Cores
Side-wall cores
Benthic Foraminifers
Side wall core
Cores
Discoaster quinqueramus
Sphaeroidinellopsis seminulina
Globigerinoides extremus
Reticulofenestra pseudoumbilica
Sphenolithus neoabies
Reticulofenestra haqii
Calcidiscus leptoporus
Globorotalia opima
Globigerina ciperoensis
Globigerina angustiumbilicata
Globigerina praebulloides
Globoquadrina venezuelana
Globorotalia permicra
Nummulites
Spiroclypeus
Operculina
Cycloclypeus
Notorotalia
Eulepidina
Nephrolepidina
Notorotalia
Miogypsinoides formosensis
Miogypsinella ubaghsi
Miogypsinoides bartamensis
Miogypsina gunteri
Miogypsina globulina
Miogypsina intermedia
Planktonic Foraminifers (N, P Zones)
Calcareous Nannofossils
Benthic Foraminiferal «Letter stage»
Stage
1200
1300
1400
1500
1600
1700
1800
UBL Cored
UBL
Sein
LBL
N20 - N17
N6
N5 - N6
N4
N4a
N4a - P22
P22 - P21
P21
P20 - P18
NN11
NN4
NN2
NN2 - NP25
NP24
NP24 - NP21
Tf1 - Te5
Te4 - Te1
Td
Tortonian
Late Miocene
Burdiga-lian
Early Miocene
Aquitanian
Undifferenciated Chattian-Aquitanian
Late Rupelian/ Early Chattian
Rupelian
Oligocene
A
Age (My)
Age/Stage
Lithostratigraphic column
Thickness (m)
Eustatic curve (Miller, 2005)
-50
0 (m)
50
Climatic events
Late Oligo-Miocene warning (1)
Mi-1 glaciation (1)
Proto-Mosoon and SAM (2)
17
18
19
20
21
22
23
24
25
26
27
28
29
30
31
32
33
Burdigalian
Aquitanian
Unid. Chattian Aqui.
Late Rup.
Rupelian
UBL cored
UBL
Sein
LBL
30
120
250
50
200
B

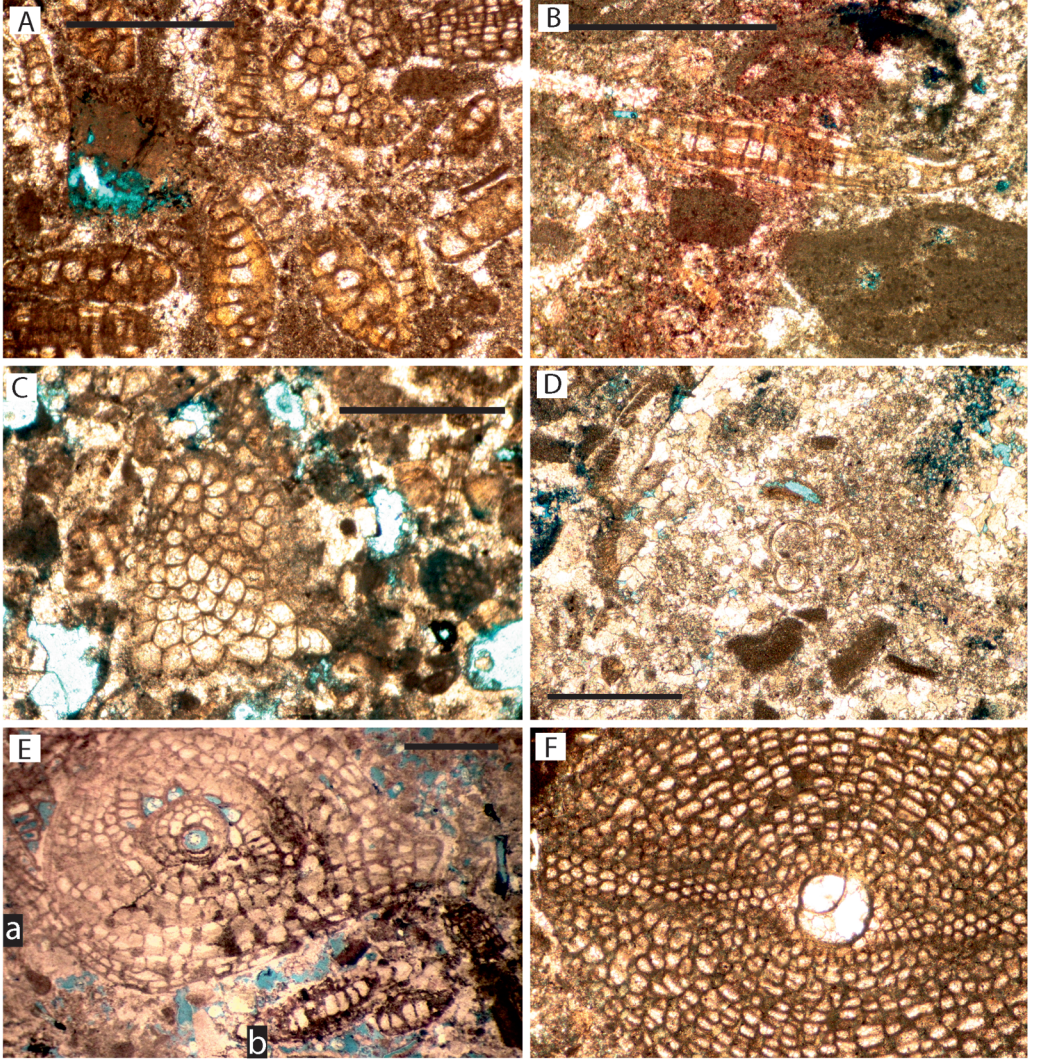
A
B
C
D
E
a
b
F

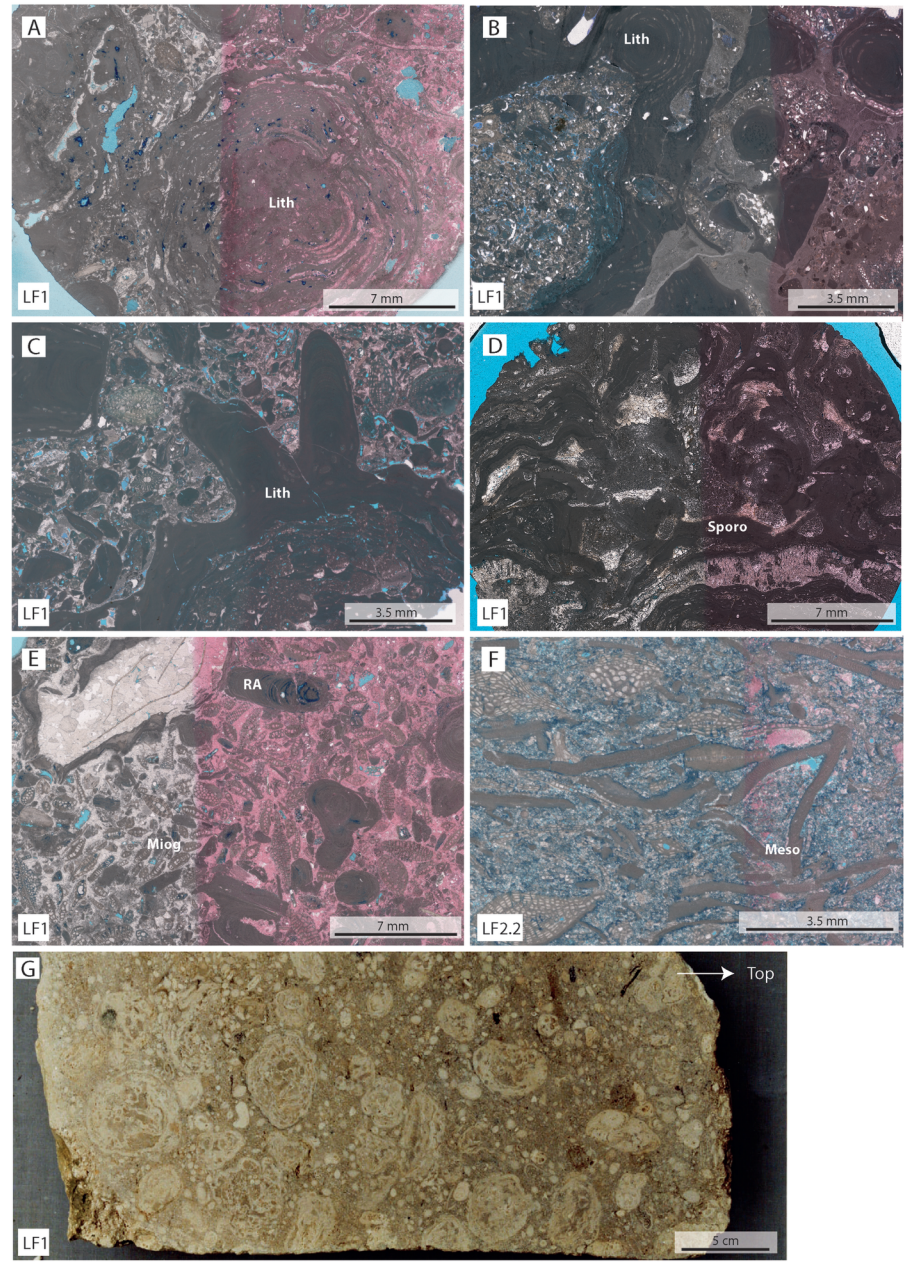
A
Lith
LF1
7 mm
B
Lith
LF1
3.5 mm
C
Lith
LF1
3.5 mm
D
Sporo
LF1
7 mm
E
RA
Miog
LF1
7 mm
F
Meso
LF2.2
3.5 mm
G
Top
LF1
5 cm

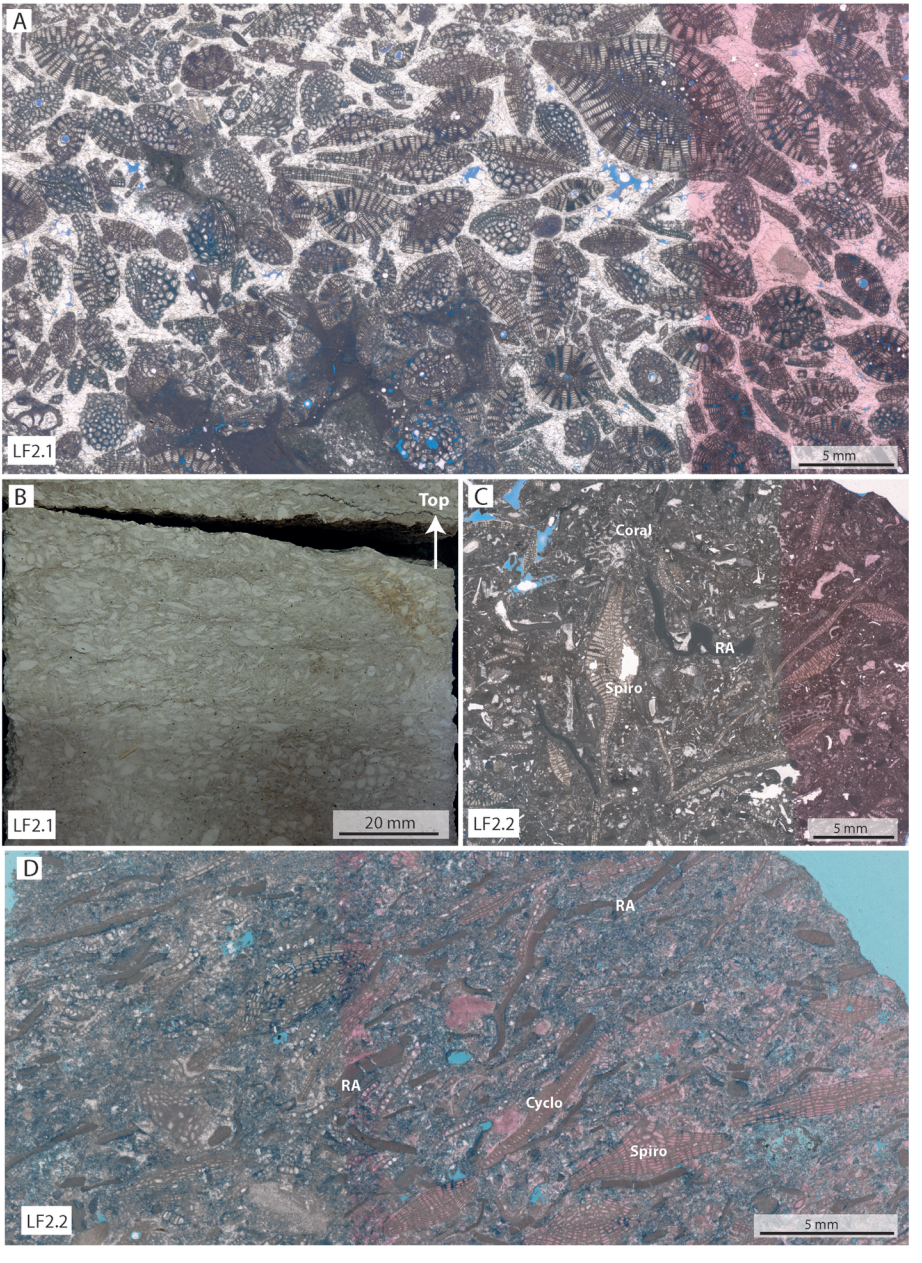
A
LF2.1
5 mm
B
Top
LF2.1
20 mm
C
Coral
RA
Spiro
LF2.2
5 mm
D
RA
RA
Cyclo
Spiro
LF2.2
5 mm

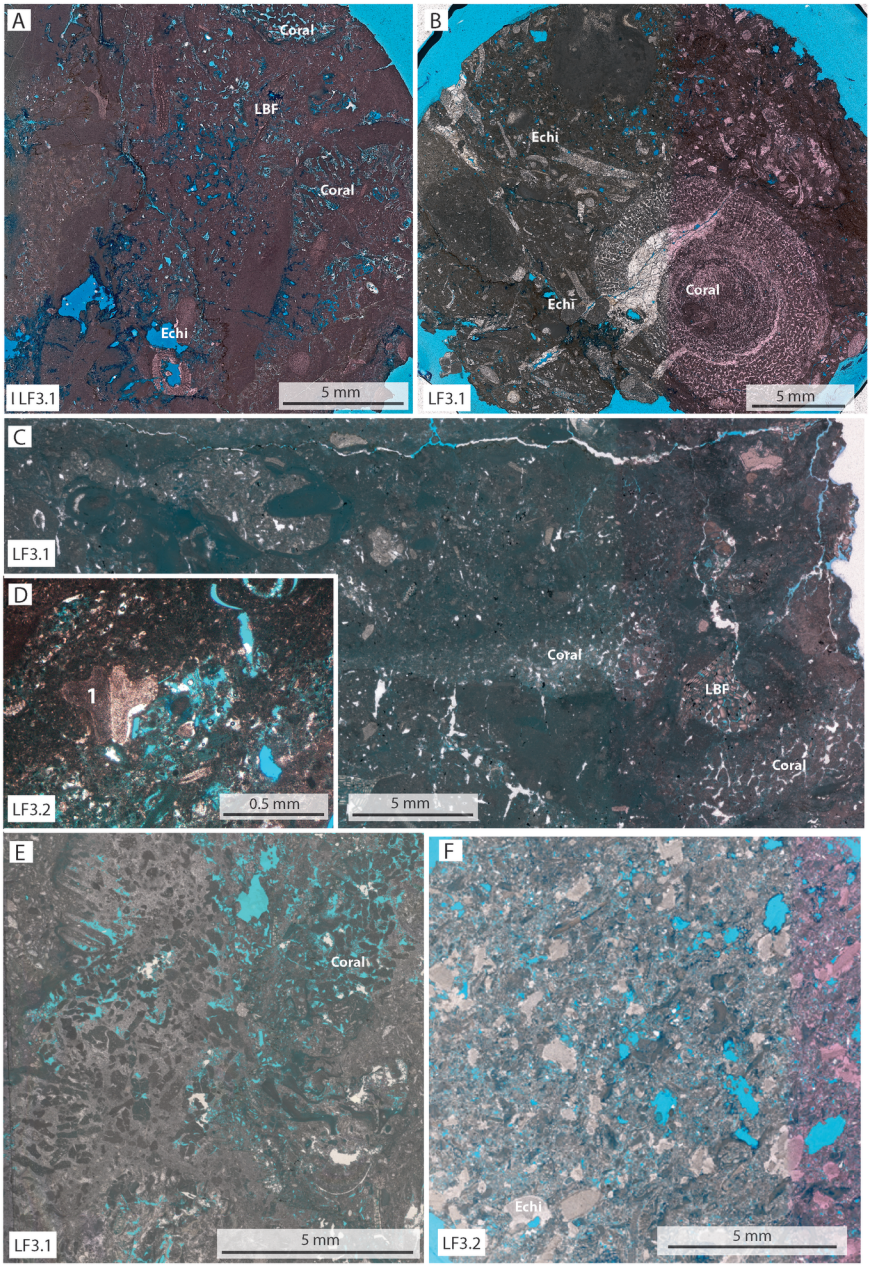
A
Coral
LBF
Coral
Echi
LF3.1
5 mm
B
Echi
Echi
Coral
LF3.1
5 mm
C
LF3.1
D
1
LF3.2
0.5 mm
Coral
LBF
Coral
5 mm
E
Coral
LF3.1
5 mm
F
Echi
LF3.2
5 mm

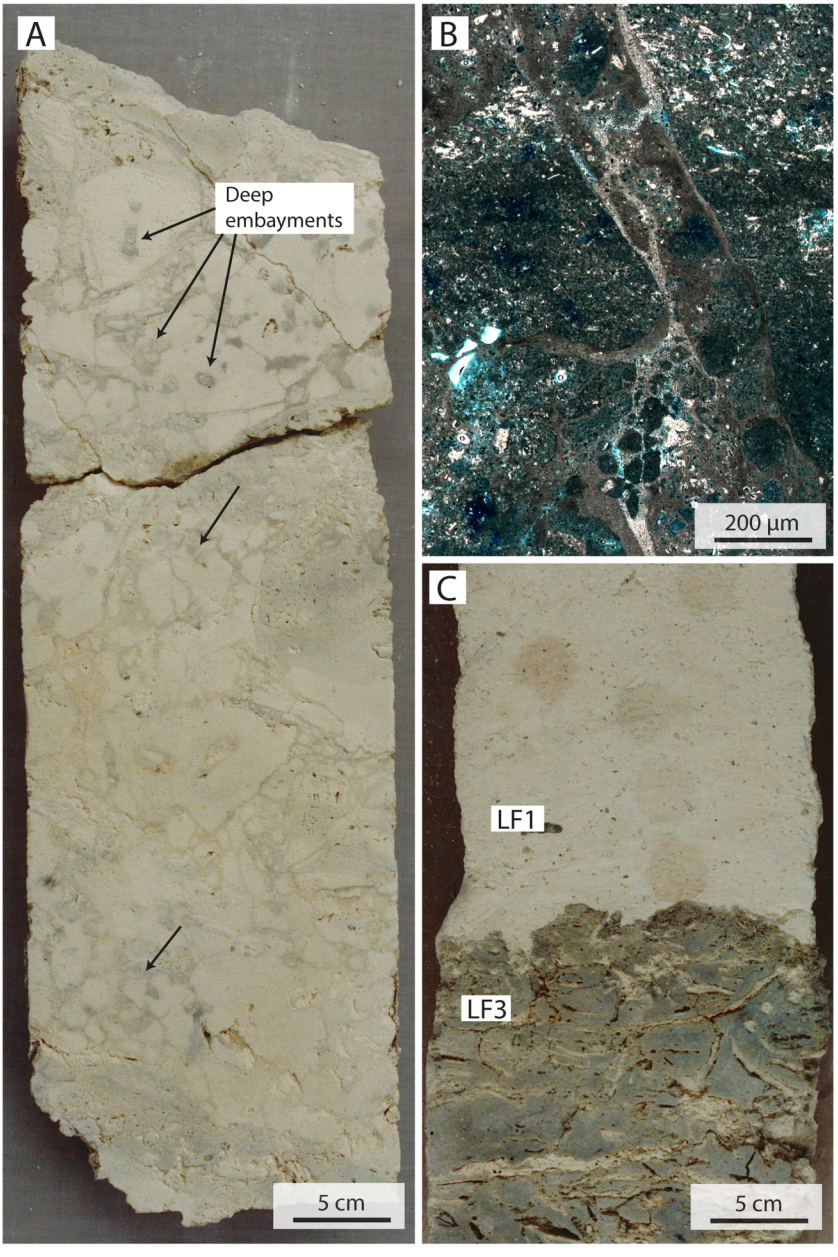
A
Deep
embayments
5 cm
B
200 µm
C
LF1
LF3
5 cm

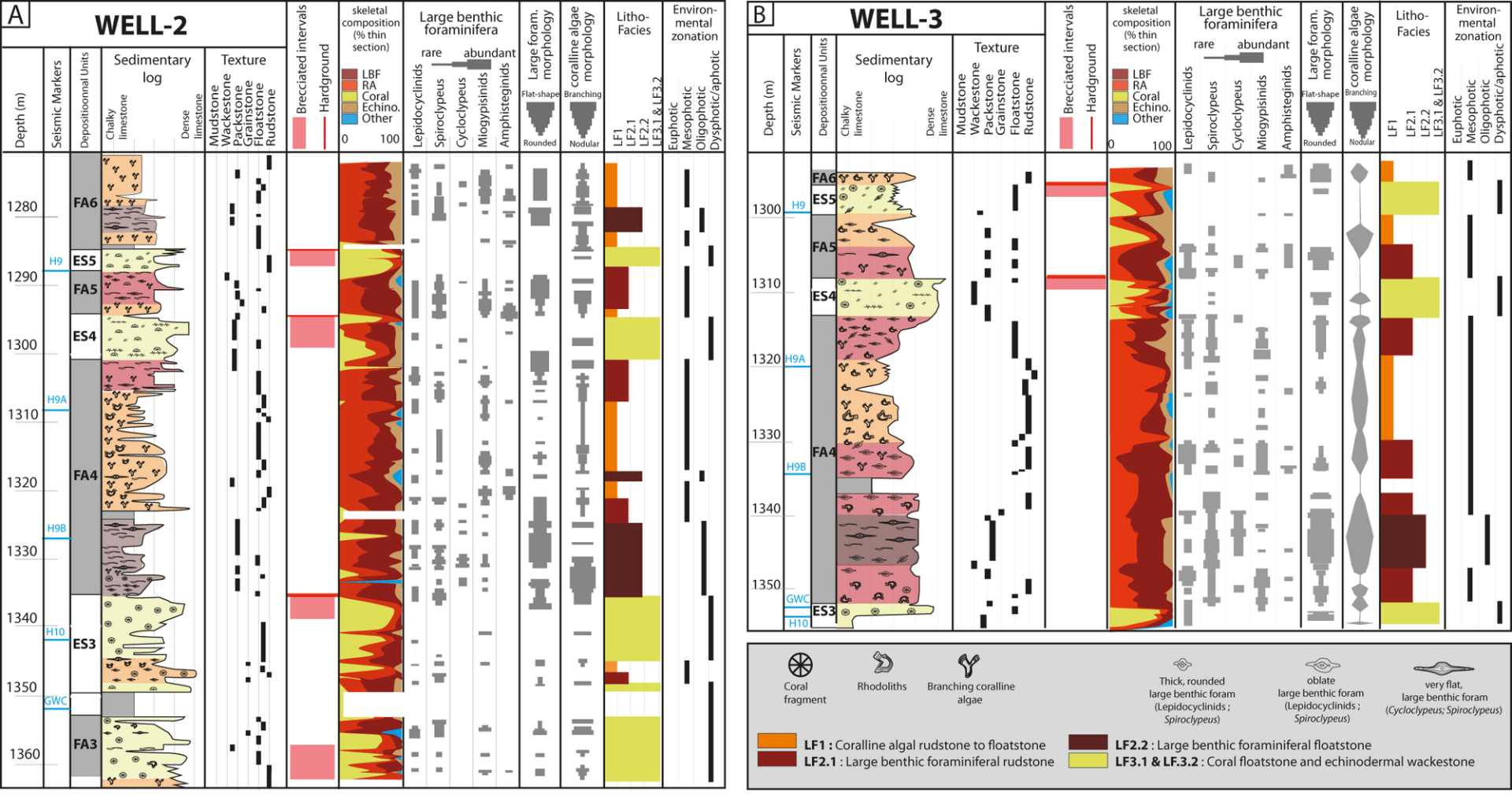
A
WELL-2
Depth (m)
Seismic Markers
Depositioonnal Units
Sedimentary log
Chalky limestone
Dense limestone
Texture
Mudstone
Wackestone
Packstone
Grainstone
Floatstone
Rudstone
Brecciated intervals
Hardground
skeletal composition (% thin section)
LBF
RA
Coral
Echino.
Other
0
100
Large benthic foraminifera
rare
abundant
Lepidocyclinids
Spiroclypeus
Cyclocypeus
Miogypisinids
Amphisteginids
Large foram. morphology
Flat-shape
Rounded
coralline algae morphology
Branching
Nodular
Litho-Facies
LF1
LF2.1
LF2.2
LF3.1 & LF3.2
Environ-mental zonation
Euphotic
Mesophotic
Oligophotic
Dysphotic/aphotic
1280
1290
1300
1310
1320
1330
1340
1350
1360
H9
H9A
H9B
H10
GWC
FA6
ES5
FA5
ES4
FA4
ES3
FA3
B
WELL-3
1300
1310
1320
1330
1340
1350
H9
H9A
H9B
GWC
H10
FA6
ES5
FA5
ES4
FA4
ES3
Coral fragment
Rhodoliths
Branching coralline algae
Thick, rounded large benthic foram (Lepidocyclinids ; Spiroclypeus)
oblate large benthic foram (Lepidocyclinids ; Spiroclypeus)
very flat, large benthic foram (Cycloclypeus; Spiroclypeus)
LF1 : Coralline algal rudstone to floatstone
LF2.1 : Large benthic foraminiferal rudstone
LF2.2 : Large benthic foraminiferal floatstone
LF3.1 & LF.3.2 : Coral floatstone and echinodermal wackestone

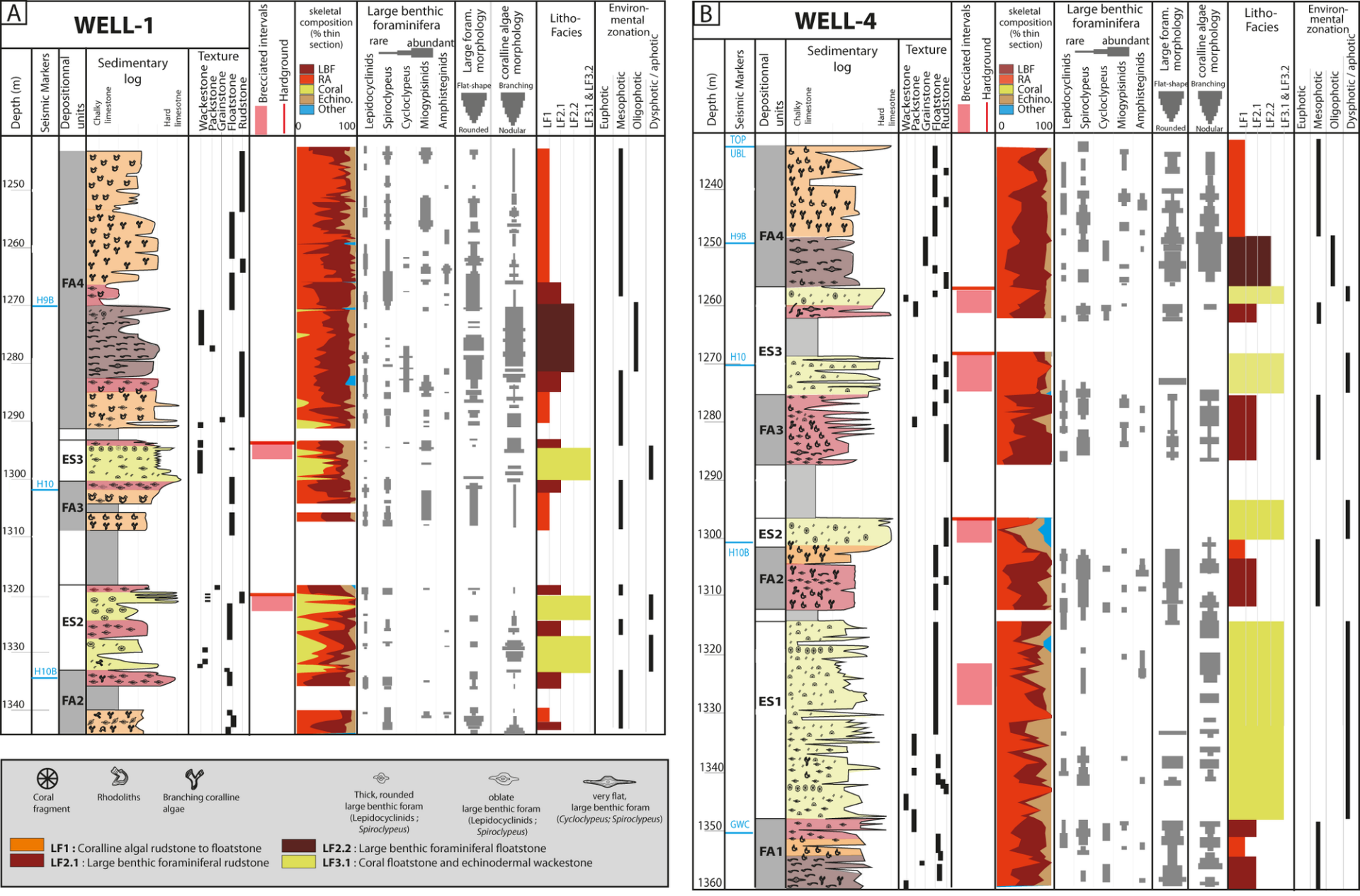
A
WELL-1
Depth (m)
Seismic Markers
Depositionnal units
Sedimentary log
Chalky limestone
Hard limestone
Texture
Wackestone
Packstone
Grainstone
Floatstone
Rudstone
Brecciated intervals
Hardground
skeletal composition (% thin section)
LBF
RA
Coral
Echino.
Other
0
100
Large benthic foraminifera
rare
abundant
Lepidocyclinids
Spiroclypeus
Cycloclypeus
Miogypisinids
Amphisteginids
Large foram. morphology
Flat-shape
Rounded
coralline algae morphology
Branching
Nodular
Litho-Facies
LF1
LF2.1
LF2.2
LF3.1 & LF3.2
Environ-mental zonation
Euphotic
Mesophotic
Oligophotic
Dysphotic / aphotic
1250
1260
1270
1280
1290
1300
1310
1320
1330
1340
H9B
H10
H10B
FA4
ES3
FA3
ES2
FA2
B
WELL-4
TOP
UBL
H9B
H10
H10B
GWC
1240
1250
1260
1270
1280
1290
1300
1310
1320
1330
1340
1350
1360
FA4
ES3
FA3
ES2
FA2
ES1
FA1
Coral fragment
Rhodoliths
Branching coralline algae
Thick, rounded large benthic foram (Lepidocyclinids ; Spiroclypeus)
oblate large benthic foram (Lepidocyclinids ; Spiroclypeus)
very flat, large benthic foram (Cycloclypeus; Spiroclypeus)
LF1 : Coralline algal rudstone to floatstone
LF2.1 : Large benthic foraminiferal rudstone
LF2.2 : Large benthic foraminiferal floatstone
LF3.1 : Coral floatstone and echinodermal wackestone

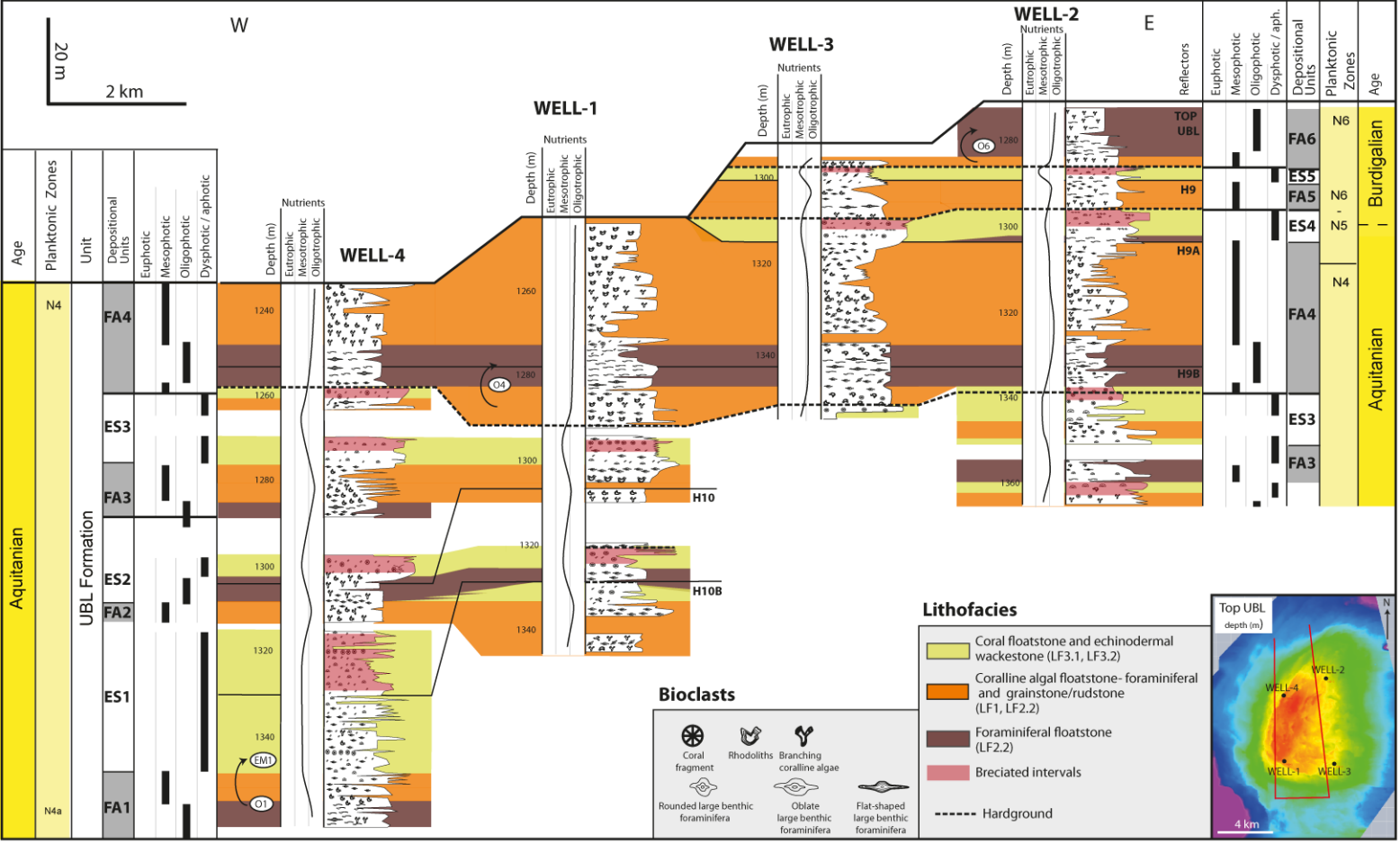
20 m
2 km
W
E
WELL-1
WELL-2
WELL-3
WELL-4
Nutrients
Eutrophic
Mesotrophic
Oligotrophic
Depth (m)
Age
Planktonic Zones
Unit
Depositional Units
Euphotic
Mesophotic
Oligophotic
Dysphotic / aphotic
Reflectors
Dysphotic / aph.
Planktonic Zones
Aquitanian
Burdigalian
N4
N4a
N6
N6 - N5
N4
UBL Formation
FA4
ES3
FA3
ES2
FA2
ES1
FA1
ES4
FA5
ES5
FA6
TOP UBL
H9
H9A
H9B
H10
H10B
O1
O4
O6
EM1
Lithofacies
Coral floatstone and echinodermal wackestone (LF3.1, LF3.2)
Coralline algal floatstone- foraminiferal and grainstone/rudstone (LF1, LF2.2)
Foraminiferal floatstone (LF2.2)
Breciated intervals
Hardground
Bioclasts
Coral fragment
Rhodoliths
Branching coralline algae
Rounded large benthic foraminifera
Oblate large benthic foraminifera
Flat-shaped large benthic foraminifera
Top UBL
depth (m)
WELL-2
WELL-4
WELL-1
WELL-3
4 km
N

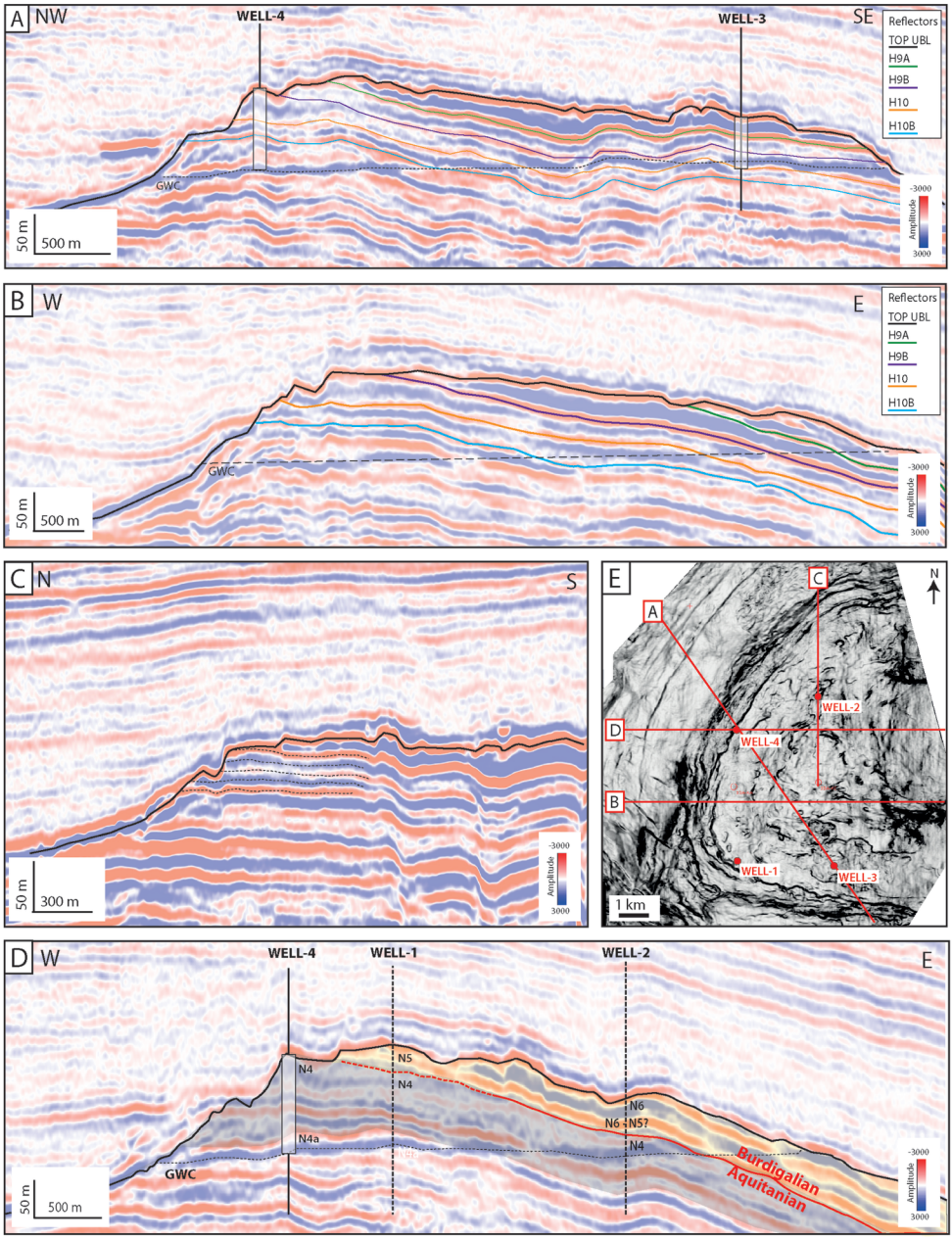
A
NW
WELL-4
WELL-3
SE
Reflectors
TOP UBL
H9A
H9B
H10
H10B
GWC
50 m
500 m
-3000
Amplitude
3000
B
W
E
C
N
S
300 m
E
C
A
D
B
WELL-2
WELL-1
1 km
D
WELL-4
WELL-1
WELL-2
N5
N4
N6
N6
N5?
N4
N4a
GWC
Burdigalian
Aquitanian

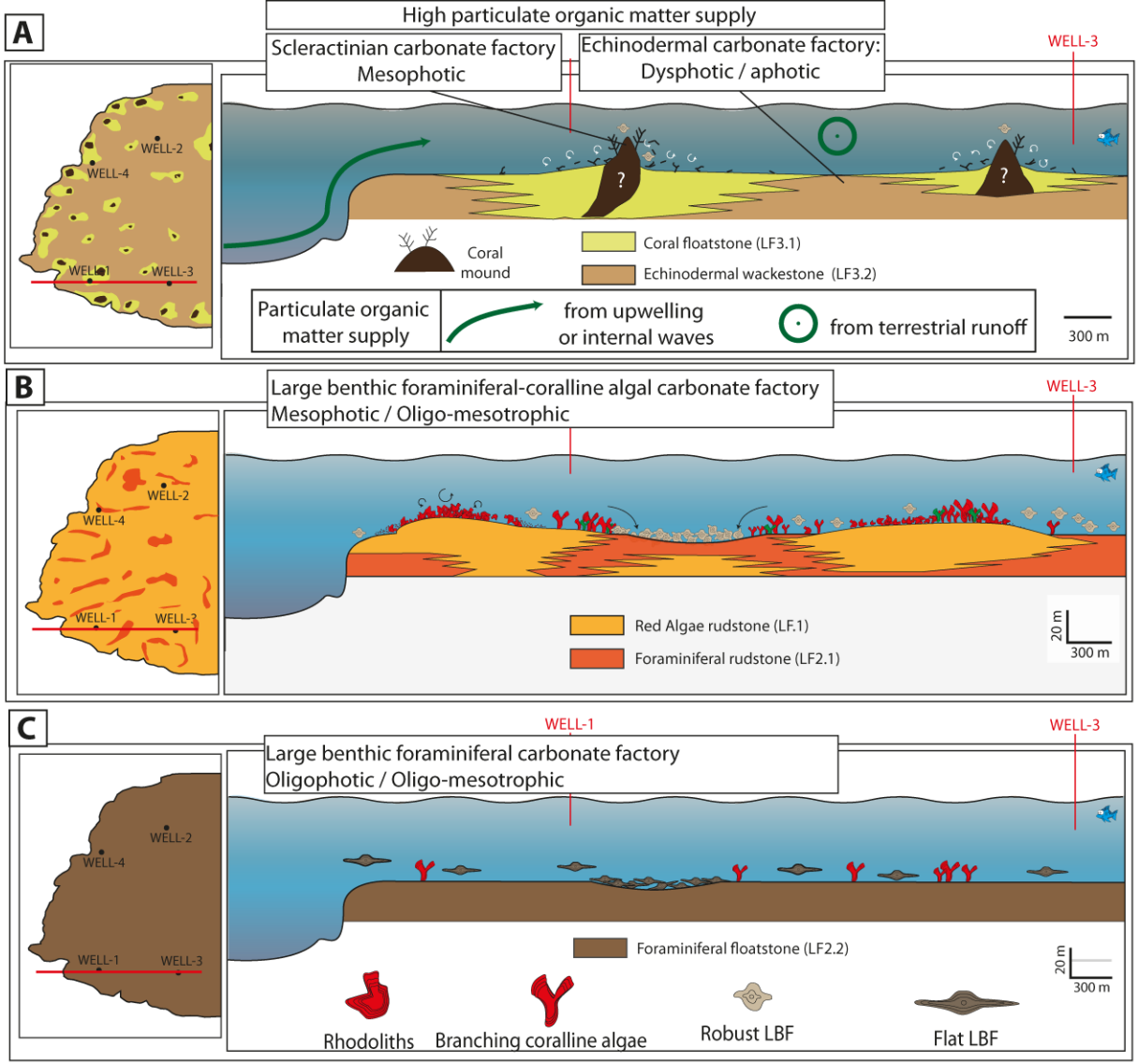

D WATER-DEPTH ESTIMATIONS

MESOPHOTIC SCLERACTINIAN CARBONATE FACTORY

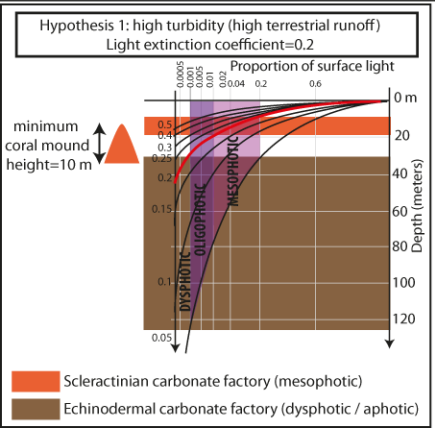

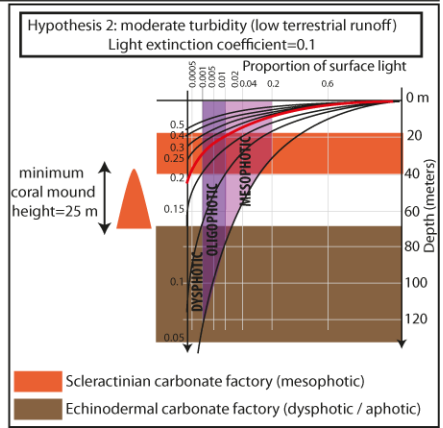

OLIGO-MESOPHOTIC CORALLINE ALGAL / FORAMINIFERAL CARBONATE FACTORY

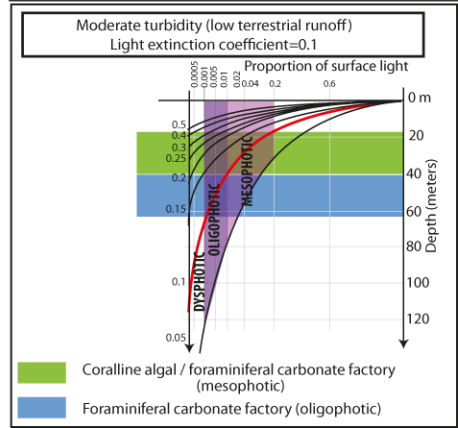

Table 1

Lithofacies, skeletal components and interpretation

	Lithofacies	Skeletal components	Interpretation
Coralline algal (LF1)	**LF1. Coralline algal floatstone to rudstone** with a coralline algal-foraminiferal wackestone to packestone matrix.	Heterometric spheroidal-ellipsoidal rhodoliths (1-10 cm in diameter) or pieces of branching coralline algae (*Lithothamnion*, *Mesophyllum* and *Sporolithon*. The foraminiferal assemblage is dominated by *Spiroclypeus tidoenganensis* and *Nephrolepidina sumatrensis,* with common occurrences of *Miogypsinoides*, *Miogypsina* and *Heterostegina (Vlerkina)*	Mesophotic zone, oligotrophic (to slightly mesotrophic) conditions, below wave-base, episodic high-energy events.
Large benthic foraminiferal dominated (LF2)	**LF2.1. Large benthic foraminiferal rudstone** with common red algal fragments. Intergranular space is occluded by sparry calcite cements.	The foraminiferal assemblage is dominated by *Lepidoclyclina (Nephrolepidina) sumatrensis, L. (N.) oneatensis*, and *Spiroclypeus tidoenganensis* with rarer specimens of *Amphistesgina, Heterostegina, Miogypsina,* and *Miogypsinoide*. Coralline algae mainly include branching and warty *Lithothamnion*, losse *Mesophyllum* and branching *Sporolithon*.	Mesophotic zone, oligotrophic (to slightly mesotrophic) conditions, below wave-base, Deposition during episodic high-energy events.
	LF2.2. Large benthic floatstone with coralline algal wackestone / packestone matrix.	Large benthic foraminifers are large (up to 2cm), thin-shelled, commonly well preserved, and typically horizontally-oriented. Dominated by *Spiroclypeus tidoenganensis* with common occurrences of *Cycloclypeus*… Laminar and loose *Mesophyllum,* together with branching *Lithothamnion* are common.	Oligophotic zone, oligotrophic (to slightly mesotrophic) conditions, below wave-base, low energy setting.
Coral dominated (LF3)	**LF3.1. Coral floatstone** With an echinodermal wackestone matrix. Coral-dominated intervals are frequently brecciated. Breccia clasts display low displacement, are sub-angular to sub-rounded in shape and exhibit common deep embayments. The space between clasts is filled with a lime mud sediment containing various proportions of small echinoderm fragments**.**	Scleractinian floatstone consists of transported fragile branches or massive fragments of *Faviids* and *Pocilloporids*. Ophiuroids, echinoids, small pieces of non-articulated coralline algae and occasional broken *Spiroclypeus* and *lepidocyclinids*.	Dysphotic to aphotic zone, below wave-base, episodic high-energy events. Bioclastic material (mainly corals) is transported and derives from an area located within mesophotic domains (coral mounds?). Breccia intervals result from the action of storms or internal waves.
	LF3.2. Echinodermal wackestone Commonly brecciated, like LF3.1	Bioclastic wackestone is dominated by echinoderm pieces including ophiuroid ossicles and echinoids, small size fragments of coralline algae. Frequently interbedded between coral floatstone LF3.1.	Dysphotic to aphotic zone, below wave-base, episodic high-energy events. Lateral equivalent of LF3.1